AMERICAN SOCIETY FOR MICROBIOLOGY | Journal of Virology®

PATHOGENESIS AND IMMUNITY

Enhanced Ability of Plant-Derived PGT121 Glycovariants To Eliminate HIV-1-Infected Cells

Sai Priya Anand,[a,b] Shilei Ding,[a] William D. Tolbert,[c] Jérémie Prévost,[a,d] Jonathan Richard,[a,d] Hwi Min Gil,[e,f] Gabrielle Gendron-Lepage,[a] Wing-Fai Cheung,[g] Haifeng Wang,[g] Rebecca Pastora,[g] Hirak Saxena,[h*] Warren Wakarchuk,[h*] Halima Medjahed,[a] Bruce D. Wines,[i,j,k] Mark Hogarth,[i,j,k] George M. Shaw,[l] Malcom A. Martin,[m] Dennis R. Burton,[n,o] Lars Hangartner,[n] David T. Evans,[e,f] Marzena Pazgier,[c] Doug Cossar,[g] Michael D. McLean,[g] Andrés Finzi[a,b,d]

[a]Centre de Recherche du CHUM, Montreal, Quebec, Canada
[b]Department of Microbiology and Immunology, McGill University, Montreal, Quebec, Canada
[c]Infectious Diseases Division, Department of Medicine of Uniformed Services University of the Health Sciences, Bethesda, Maryland, USA
[d]Département de Microbiologie, Infectiologie, et Immunologie, Université de Montréal, Montreal, Quebec, Canada
[e]Wisconsin National Primate Research Center, University of Wisconsin, Madison, Wisconsin, USA
[f]Department of Pathology and Laboratory Medicine, University of Wisconsin—Madison, Madison, Wisconsin, USA
[g]PlantForm Corporation, Toronto, Ontario, Canada
[h]Department of Chemistry and Biology, Ryerson University, Toronto, Ontario, Canada
[i]Immune Therapies Group, Burnet Institute, Melbourne, VIC, Australia
[j]Department of Clinical Pathology, University of Melbourne, Melbourne, VIC, Australia
[k]Department of Immunology and Pathology Monash University, Melbourne, VIC, Australia
[l]Departments of Medicine and Microbiology, Perelman School of Medicine, University of Pennsylvania, Philadelphia, Pennsylvania, USA
[m]Laboratory of Molecular Microbiology, National Institute of Allergy and Infectious Diseases, National Institutes of Health, Bethesda, Maryland, USA
[n]Department of Immunology and Microbiology, The Scripps Research Institute, La Jolla, California, USA
[o]Ragon Institute of Massachusetts General Hospital, Massachusetts Institute of Technology, Harvard University, Cambridge, Massachusetts, USA

Sai Priya Anand and Shilei Ding contributed equally to this article. Author order was determined alphabetically.

ABSTRACT The activity of broadly neutralizing antibodies (bNAbs) targeting HIV-1 depends on pleiotropic functions, including viral neutralization and the elimination of HIV-1-infected cells. Several *in vivo* studies have suggested that passive administration of bNAbs represents a valuable strategy for the prevention or treatment of HIV-1. In addition, different strategies are currently being tested to scale up the production of bNAbs to obtain the large quantities of antibodies required for clinical trials. Production of antibodies in plants permits low-cost and large-scale production of valuable therapeutics; furthermore, pertinent to this work, it also includes an advanced glycoengineering platform. In this study, we used *Nicotiana benthamiana* to produce different Fc-glycovariants of a potent bNAb, PGT121, with near-homogeneous profiles and evaluated their antiviral activities. Structural analyses identified a close similarity in overall structure and glycosylation patterns of Fc regions for these plant-derived Abs and mammalian cell-derived Abs. When tested for Fc-effector activities, afucosylated PGT121 showed significantly enhanced FcγRIIIa interaction and antibody dependent cellular cytotoxicity (ADCC) against primary HIV-1-infected cells, both *in vitro* and *ex vivo*. However, the overall galactosylation profiles of plant PGT121 did not affect ADCC activities against infected primary $CD4^+$ T cells. Our results suggest that the abrogation of the Fc N-linked glycan fucosylation of PGT121 is a worthwhile strategy to boost its Fc-effector functionality.

IMPORTANCE PGT121 is a highly potent bNAb and its antiviral activities for HIV-1 prevention and therapy are currently being evaluated in clinical trials. The importance of its Fc-effector functions in clearing HIV-1-infected cells is also under investigation. Our results highlight enhanced Fc-effector activities of afucosylated PGT121 MAbs that could be important in a therapeutic context to accelerate infected cell clearance and slow disease

Citation Anand SP, Ding S, Tolbert WD, Prévost J, Richard J, Gil HM, Gendron-Lepage G, Cheung W-F, Wang H, Pastora R, Saxena H, Wakarchuk W, Medjahed H, Wines BD, Hogarth M, Shaw GM, Martin MA, Burton DR, Hangartner L, Evans DT, Pazgier M, Cossar D, McLean MD, Finzi A. 2021. Enhanced ability of plant-derived PGT121 glycovariants to eliminate HIV-1-infected cells. J Virol 95:e00796-21. https://doi.org/10.1128/JVI.00796-21.

Editor Viviana Simon, Icahn School of Medicine at Mount Sinai

Address correspondence to Andrés Finzi, andres.finzi@umontreal.ca.

* Present address: Hirak Saxena, Department of Biological Sciences, University of Alberta, Edmonton, Alberta, Canada; Warren Wakarchuk, Department of Biological Sciences, University of Alberta, Edmonton, Alberta, Canada.

Received 10 May 2021
Accepted 25 June 2021
Accepted manuscript posted online 7 July 2021
Published 25 August 2021

progression. Future studies to evaluate the potential of plant-produced afucosylated PGT121 in controlling HIV-1 replication *in vivo* are warranted.

KEYWORDS HIV-1, Env glycoproteins, broadly neutralizing antibodies, PGT121, plant antibodies, *Nicotiana benthamiana*, glycosylation, fucose, galactose, ADCC, FcγRIIIa, Envelope glycoproteins, HIV-1, plant antibodies, neutralizing antibodies

Human immunodeficiency virus type 1 (HIV-1) envelope glycoproteins (Env) represent the main virus-specific antigen exposed at the surface of viral particles and infected cells. As such, Env represents a unique target for neutralization and Fc-effector functions, such as antibody-dependent cellular cytotoxicity (ADCC). Several *in vivo* studies in humanized mice and nonhuman primate (NHP) models of HIV-1 infection (1–7), as well as in HIV-1-infected humans, have shown that passive administration of broadly neutralizing antibodies (bNAbs) can confer both effective preexposure prophylaxis and therapeutic control of viremia (8–12). The progress made over the last few years further spurred the interest to use bNAbs for protection and control of HIV-1 infection in ongoing clinical trials (NCT03707977, NCT04319367, and NCT03837756). With the expansion in the use of bNAbs and the large amounts of antibodies required to perform these studies, the cost that is associated with producing them in mammalian cells poses a significant barrier (13, 14). Alternate cost-effective platforms to express and purify these bNAbs are being explored. Strategies that are currently being tested to increase the production of monoclonal antibody (MAb) therapeutics include bacteria such as *Escherichia coli* (15) and yeast such as *Pichia pastoris* (16).

Another platform gaining significant interest in the recent decade is the production of MAbs and other biologic drugs in plant-based systems using *Nicotiana benthamiana* (17, 18). This allows the unlimited potential for large-scale, cost-effective production of valuable therapeutic proteins (19, 20). In addition, production cost is not the only advantage of this technology. This method offers rapid development timelines since plant expression systems apply transient-expression technology using *Agrobacterium* to introduce DNA expression vectors encoding MAbs of interest into the plant by horizontal gene transfer. This system allows MAb production of upwards of 10% total soluble protein biomass that usually peaks within 1 week, after which the plants can be harvested for product purification (21, 22).

Furthermore, plant expression systems now also harbor the advantage of an advanced glycoengineering platform (23). Since posttranslational modifications are critical for the functional activities of antibodies, glycoengineering is a valuable tool to improve their Fc-effector functions. Glycoengineered MAbs have already demonstrated their potential for other viral infections, including Zika (24), Dengue (25), rabies (26) and West Nile (27) viruses. The glycosylation status of MAbs modulates Fc gamma receptors (FcγR) binding to improve or decrease Ab-mediated effector functions, such as ADCC. This is dictated by glycan moieties that can be added or removed from asparagine-297 (N297), the single N-linked glycosylation site of IgG Fc fragment. Mutations of N297 residue have been shown to diminish FcγR binding and specific Fc-glycan modifications have been shown to modulate Ab functionality (28–31). Concurrent with the research being done to glycoengineer Env-specific bNAbs against HIV-1 (32–35), we have utilized a *N. benthamiana*-based glycoengineering platform in this study that is valuable in the currently expanding field of HIV-1 bNAbs therapy.

Here, we generated different glycoforms of the highly potent PGT121 bNAb, which recognizes the N332 supersite at the base of Env V3 loop (36–40). PGT121 has been shown to provide prolonged viral suppression in chronically infected rhesus macaques (1) and to mediate effective protection against cell-free viral mucosal (41, 42) and cell-associated intravenous (43) SHIV challenges. While bNAbs antiviral effects can be largely attributed to the ability of antibodies to neutralize viral particles (44), Fc-mediated functions have also been associated with optimal bNAb activity *in vivo* (1, 2, 45–48) but remains somewhat controversial in the context of protection against infection (49). We evaluated the abilities of these PGT121 glycovariants to interact with FcγRIIIa and mediate efficient ADCC against HIV-1 and SHIV-infected cells *in vitro* and *ex vivo*.

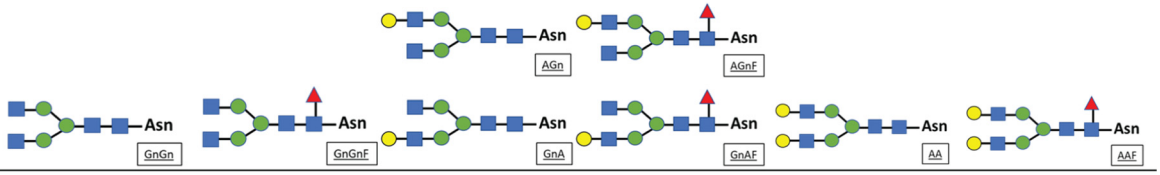

PGT121 G0	**69%**					
PGT121 G0F	12%	**66%**				
PGT121 G2	8%		9%		**42%**	
PGT121 G2F	2%	10%	11%	8%	8%	**42%**

GlcNAc **Fucose** **Galactose** **Mannose**

FIG 1 N-linked glycans of *N. benthamiana*-produced PGT121 glycovariants. The percentages of predominant N-glycosylations on PGT121 G0, PGT121 G0F, PGT121 G2, and PGT121 G2F are presented in the table. Schematic diagrams are across the top, where Asn is asparagine 297, GnGn is diantennary *N*-acetylglucosamine, F is fucose, and A is galactose. Glycan species abundances are given as percentages, and minor glycoforms are not indicated. Glycan nomenclature is further described by ProGlycAn.

RESULTS

Generation of near-homogeneous plant-derived PGT121 glycovariants. Most therapeutic protein drugs, such as MAbs, exist as mixtures of glycoproteins that are identical in amino acid sequence composition yet variable in glycosylation profile due to a series of posttranslational modifications. In this study, a versatile platform was used to produce Env-specific bNAb PGT121 with controlled posttranslational glycomodification. This platform involved transient expression of antibody genes in a proprietary *Nicotiana benthamiana* plant line engineered for knockdown of plant-specific α1,3-fucosylation and β1,2-xylosylation (KDFX) (18), thus producing MAbs with predominantly biantennary *N*-acetylglucosamine (GnGn) glycans (G0 glycoform). When MAbs were transiently coexpressed with human α-1,6 fucosyltransferase in KDFX plants, glycans bearing core fucose resulted; with human α1,4 galactosyltransferase, glycans with galactose linkages being either mono- or diantennary resulted (50, 51). In this study, we produced diverse PGT121 glycovariants that were purified from different plant treatments, resulting in mainly G0 (agalactosylated and afucosylated), G0F (agalactosylated and fucosylated), G2 (two galactose residues and afucosylated) or G2F (two galactose residues and fucosylated) glycans (Fig. 1), respectively, with minor amounts of branched oligomannose residues. All plant treatments produced antibodies with highly homogeneous glycosylation profiles characterized by a single dominant glycan. MAb PGT121 produced in mammalian 293F cells was also used in this study; its glycosylation status has been previously reported as G0F (agalactosylated and fucosylated) with minor amounts of other N-linked glycans (42).

Fc glycosylation does not affect the ability of PGT121 to recognize infected cells nor its neutralization capacity. Taking our panel of glycoengineered PGT121 MAbs, we first evaluated their overall binding capacity to Env on the surface of infected cells compared to the 293F-produced PGT121. First, we used a lymphocytic cell line (CEM.NKr) infected with three different infectious molecular clones (IMCs) expressing Env in its "closed" conformation (HIV-1_{JRCSF} [52], $SHIV_{AD8\text{-}EO}$ [53], and $SHIV_{BG505}$ N332 S375Y [44]). As controls, we included a version of 293F-produced PGT121 with Fc mutations known to decrease FcγRIIIa interactions (L234A/L235A [LALA]), as well as a nonspecific MAb, trastuzumab, a HER2-specific MAb used in specific cancer immunotherapies (54) in our panel. At 2 days postinfection, cells were stained with the respective MAbs, and all plant-produced PGT121 glycovariants recognized cells infected with the three IMCs to the same extent as 293F-produced PGT121 (Fig. 2A to C). Furthermore, in agreement with an equivalent Env recognition by all PGT121 glycovariants, no significant differences in their ability to neutralize HIV-1_{JRCSF}, $SHIV_{AD8\text{-}EO}$, and $SHIV_{BG505}$ lentiviral particles were observed (Fig. 2D to F). These results confirm that modifying the Fc domain does not affect the antigen recognition and neutralization capabilities of PGT121.

The Fc glycosylation profile of PGT121 regulates its capacity to mediate ADCC. Next, we evaluated the efficacy of our panel of glycoengineered MAbs to eliminate infected cells.

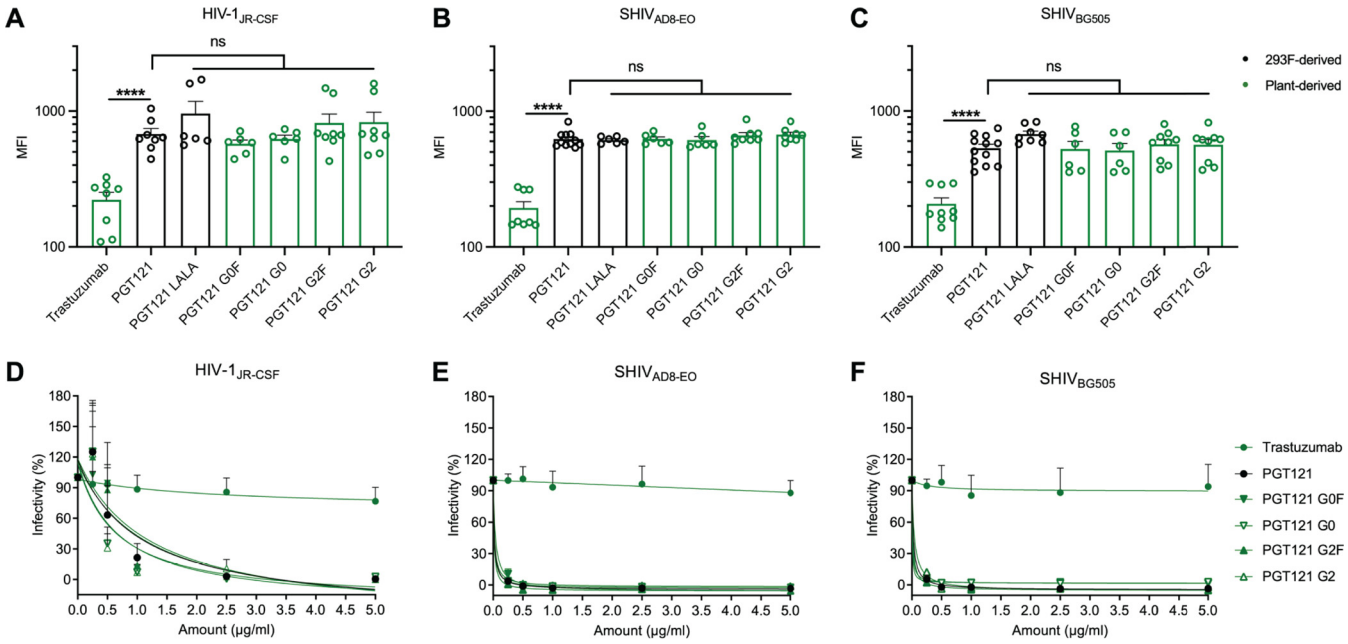

FIG 2 Fc glycosylation does not affect the ability of PGT121 to recognize infected cells or its neutralization capacity. Cell surface staining of CEM.NKr CCR5$^+$ cells infected with HIV-1$_{JRCSF}$ (A), SHIV$_{AD8-EO}$ (B), and SHIV$_{BG505}$ (C) was performed 48 h postinfection. Antibody binding was detected using Alexa Fluor 647-conjugated anti-human secondary Abs. Graphs represent the median fluorescence intensities (MFI) in the infected population (p24+ or p27+) determined from at least five independent experiments, with the error bars indicating means ± the standard errors of the mean (SEM). Statistical significance was tested using an unpaired *t* test or a Mann-Whitney U test based on statistical normality (****, $P < 0.0001$; ns, nonsignificant). (D to F) Lentiviral particles produced from HIV-1$_{JRCSF}$ (D), SHIV$_{AD8-EO}$ (E), and SHIV$_{BG505}$ (F) IMCs. Viruses were incubated with serial dilutions of trastuzumab and PGT121 MAbs at 37°C for 1 h prior to infection of TZM-bl target cells. The infectivity at each Ab concentration tested is shown as the percentage of infection without Ab for each virus. Quadruplicate samples were analyzed in each experiment. The data shown are the means of results obtained in at least three independent experiments. Error bars indicate means ± the SEM. Black histogram/curves represent 293F cell-derived MAbs and green histogram/curves represent plant-derived MAbs.

The susceptibility of CEM.NKR cells (infected HIV-1$_{JRCSF}$, SHIV$_{AD8-EO}$, and SHIV$_{BG505}$) to ADCC was measured with a previously described fluorescence-activated cell sorting (FACS)-based ADCC assay that measures the elimination of productively infected cells by measuring the presence of intracellular HIV-1 or SHIV capsid antigens (p24+ and p27+, respectively) (44, 55, 56) (Fig. 3A to C). As expected, no ADCC activity was observed with the negative control, trastuzumab. Furthermore, the capacity of PGT121 to mediate ADCC was significantly impaired by the introduction of the LALA mutations in its Fc domains. Despite equivalent recognition of Env (Fig. 2), we observed significant differences in the abilities of the different PGT121 glycovariants to mediate ADCC. As expected, the plant-produced agalactosylated and fucosylated PGT121 (PGT121 G0F) gave results similar to those for 293F-produced PGT121, where the N-linked glycans are also predominantly G0F. Although significant increases in ADCC activities were observed with the two afucosylated PGT121 MAbs (G0 and G2) compared to their fucosylated counterparts (G0F and G2F), the galactosylated MAb (PGT121 G2) harbored the most potent activity against CEM.NKR cells infected with HIV-1$_{JRCSF}$ (Fig. 3A). In contrast, no effect of galactosylation was seen against both SHIV-infected cells.

We confirmed the enhanced ADCC activity of galactosylated PGT121 using a different luciferase based ADCC assay that also relies on the specific elimination of infected cells (57). In this assay, infected CEM.NKR-CCR5-sLTR-Luc cells expressing a Tat-driven luciferase reporter gene serve as target cells, while a CD16$^+$ NK cell line is used as effector cells (57–59). Since luciferase is only expressed upon productive infection, elimination of infected cells can be calculated by the loss of luciferase activity. As expected, similar results were obtained with this assay, where the afucosylated MAb (PGT121 G2) had enhanced ADCC activity compared to the fucosylated MAb (PGT121 G2F) (Fig. 3D and E).

The Fc glycosylation profile of PGT121 modulates FcγRIIIa interaction and ADCC against infected primary CD4$^+$ T cells. To assess the activities of *N. benthamiana*-derived PGT121 MAbs in a more physiological setting, we aimed to validate our results obtained

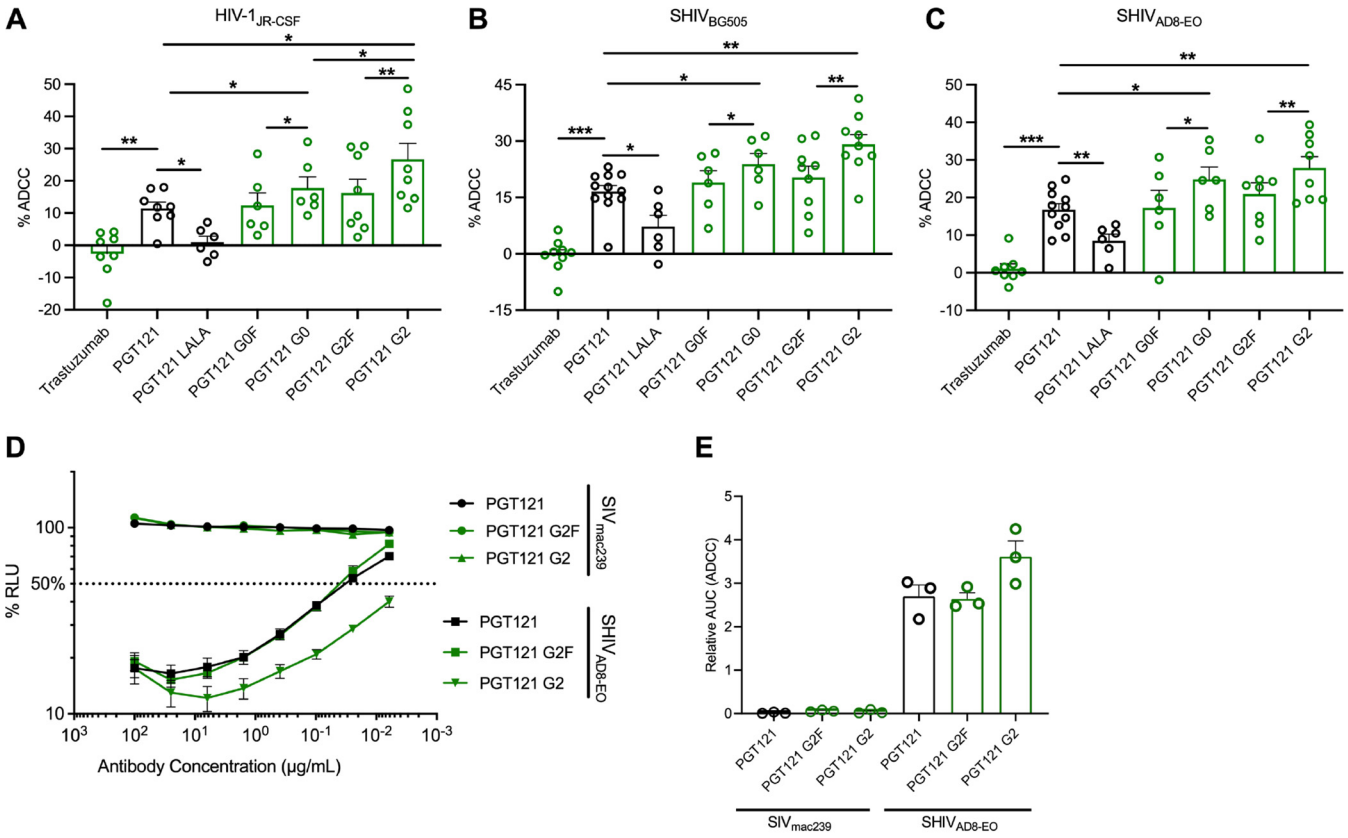

FIG 3 Fc glycosylation profile of PGT121 regulates its ADCC capacity against infected cells. CEM.NKR-CCR5-sLTR-Luc cells infected with HIV-1_{JRCSF} (A), $SHIV_{BG505}$ (B), and $SHIV_{AD8-EO}$ (C) were used as target cells. PBMCs from uninfected donors were used as effector cells in a FACS-based ADCC assay. The graphs shown represent the percentages of ADCC obtained in the presence of the respective antibodies. (D and E) For the luciferase assay, CEM.NKr-CCR5-sLTR-Luc cells infected with $SHIV_{AD8-EO}$, or SIV_{mac239} as a negative control. ADCC responses were measured as the dose-dependent loss of luciferase activity in RLU after incubation of infected CEM.NKR-CCR5-sLTR-Luc cells with $CD16^+$ KHYG-1 effector cells in the presence of antibody. Values are the means ± standard deviations (error bars) for triplicate wells, and the dotted line indicates half-maximal lysis of infected cells. (E) Area under the curve (AUC) values were calculated using from curves of increasing MAb concentrations shown in panel D. Error bars indicate means ± the SEM. Statistical significance was tested using a paired *t* test or Wilcoxon matched-pairs signed-rank test based on statistical normality (*, $P < 0.05$; **, $P < 0.01$; ***, $P < 0.001$). Black histogram bars represent 293F cell-derived MAbs and green histogram bars represent plant-derived MAbs.

using infected CEM.NKr cell line with infected primary $CD4^+$ T cells (Fig. 4). We purified primary $CD4^+$ T lymphocytes from resting peripheral blood mononuclear cells (PBMCs) by negative selection and activated them with PHA-L/IL-2, followed by infection with HIV-1_{JRCSF}, $SHIV_{AD8-EO}$, or $SHIV_{BG505}$. Once again, all our plant-produced PGT121 glycovariants recognized cells infected with the three viruses to the same extent as the 293F-produced PGT121 (Fig. 4A to C).

The N-linked glycosylation profile of IgG Fc portion has been described to strongly dictate their ability to interact with FcγRs (28, 60). To further evaluate the impact of PGT121 glycoforms on its interaction with FcγRIIIa, we incubated antibody-opsonized infected primary $CD4^+$ T cells with a soluble recombinant dimeric FcγRIIIa protein that models the cross-linking of FcγRs by Abs, a process essential to activate effector cells (61–63). Despite equivalent recognition of Env, the fucosylated PGT121 MAbs had decreased dimeric FcγRIIIa engagement compared to the afucosylated glycoforms (Table 1 and Fig. 4D to F). Moreover, both agalactosylated and galactosylated MAbs (PGT121 G0 and G2, respectively) had equivalent binding of FcγRIIIa in cells infected with all three viruses tested (Fig. 4D to F).

To evaluate whether the engagement of FcγRIIIa translates to ADCC, primary $CD4^+$ T cells from different healthy uninfected donors were infected with HIV-1_{JRCSF} and investigated for their ADCC susceptibility in the presence of autologous effector cells. Similar ADCC responses were observed with significant enhancements in the presence of the two afucosylated MAbs (PGT121 G0 and G2) (Table 1 and Fig. 4G). Akin to the engagement of FcγRIIIa, the presence or absence of galactose did not impact ADCC responses. Moreover, the overall

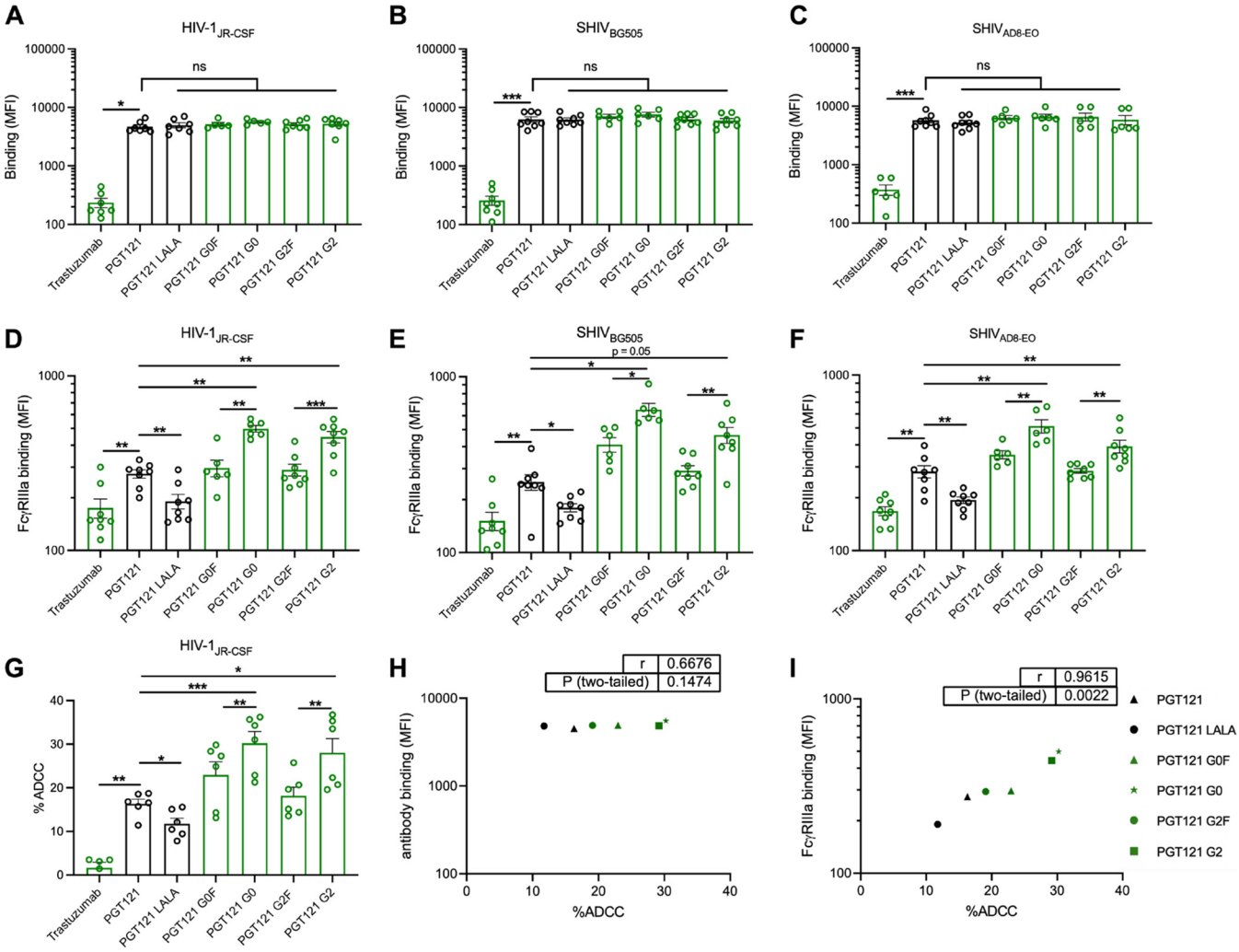

FIG 4 Fc glycosylation profile of PGT121 modulates FcγRIIIa interaction and ADCC against infected primary CD4$^+$ T cells. Cell surface staining of primary CD4$^+$ T cells infected with (A and D) HIV-1$_{JRCSF}$, (B and E) SHIV$_{AD8\text{-}EO}$, and (C and F) SHIV$_{BG505}$ was performed 48 h postinfection. Antibody binding was detected either by using Alexa Fluor 647-conjugated anti-human secondary Abs (A to C) or by using biotin-tagged dimeric rsFcγRIIIa (0.2 μg/ml) followed by the addition of Alexa Fluor 647-conjugated streptavidin (D to F). (A to F) Graphs represent MFI values in the infected population (p24+ or p27+) determined from at least five independent experiments, with the error bars indicating means ± the SEM. (G) Primary CD4$^+$ T cells infected with HIV-1$_{JRCSF}$ were used as target cells. Autologous PBMCs were used as effector cells in a FACS-based ADCC assay. The graph represents the percentages of ADCC obtained in the presence of the respective antibodies. Statistical significance was tested using a paired *t* test or Wilcoxon matched-pairs signed-rank test based on statistical normality (*, $P < 0.05$; **, $P < 0.01$; ***, $P < 0.001$; ns, nonsignificant). Black histogram bars represent 293F cell-derived MAbs, and green histogram bars represent plant-derived MAbs. (H and I) Correlations between the levels of ADCC and levels of antibody binding (H) or FcγRIIIa binding (I), as measured on primary CD4$^+$ T cells infected with HIV-1$_{JRCSF}$. Statistical significance was tested using a Pearson correlation test. Black points represent 293F cell-derived MAbs, and green points represent plant-derived MAbs.

capacity of our panel of PGT121 glycoforms to recognize Env did not correlate with the differences in ADCC responses observed ($r = 0.6676$, $P = 0.1474$) (Fig. 4H), while their ability to interact with the dimeric FcγRIIIa correlated significantly with ADCC activity exhibited against HIV-1$_{JRCSF}$-infected primary CD4$^+$ T cells ($r = 0.9615$, $P = 0.0022$) (Fig. 4I). Thus, the enhanced ADCC functionality observed with the afucosylated PGT121 MAbs appears to depend on their improved capacity to interact with FcγRIIIa.

Susceptibility of *ex vivo*-expanded primary CD4$^+$ T cells from HIV-1-infected individuals to PGT121-mediated ADCC. Since our results indicate that Fc fucosylation of PGT121 plays an important role in modulating FcγRIIIa interaction and ADCC response efficacy, we further evaluated whether our panel of plant-derived PGT121 glycovariants were able to eliminate *ex vivo*-expanded endogenously infected CD4$^+$ T cells. We isolated primary CD4$^+$ T cells from four antiretroviral therapy (ART)-treated HIV-1-infected individuals and activated them with PHA-L/IL-2, where viral replication

TABLE 1 Functionalities of PGT121 glycovariants targeting HIV-1_{JRCSF}-infected primary $CD4^+$ T cells[a]

Parameter	Trastuzumab†	PGT121*	PGT121 LALA*	PGT121 G0F†	PGT121 G0†	PGT121 G2F†	PGT121 G2†
Antibody binding	0.05	1.00	1.06	1.10	1.20	1.10	1.12
FcγRIIIa binding	0.64	1.00	0.70	1.18	1.82	1.05	1.63
%ADCC	0.10	1.00	0.72	1.39	1.85	1.12	1.72

[a]Ab binding, FcγRIIIa binding, and ADCC were measured as described in Materials and Methods. Respective values obtained for each assay are normalized to the value obtained by PGT121. *, 293F-derived MAbs; †, plant-derived MAbs.

was followed by intracellular p24 staining. In agreement with the results obtained with HIV-1_{JRCSF}-infected primary $CD4^+$ T cells, endogenously infected primary $CD4^+$ T cells were also more susceptible to ADCC mediated by afucosylated PGT121 MAbs. Similarly, these MAbs were also able to engage with the dimeric FcγRIIIa more efficiently than the fucosylated PGT121, despite their comparable binding to Env present on the surface of infected cells (Fig. 5).

The Fc regions of *N. benthamiana*-derived and mammalian cell-derived PGT121 are structurally similar with differences in N297 sugar composition. Functional characterizations of our panel of glycoengineered PGT121 MAbs demonstrated significant differences in Fc-mediated effector activities compared to mammalian cell derived PGT121. To understand whether there are any differences in the overall structure and glycosylation pattern within the Fc region of our engineered MAbs we determined the 2.6-Å and 2.1-Å crystal structures of *N. benthamiana*-expressed galactosylated afucosylated (G2) and fucosylated (G2F) PGT121 Fcs, respectively (Table 2 and Fig. 6). Both Fcs crystallized in the same $P2_12_12_1$ space group with similar dimensions (Table 2) indicative of their close structural similarity. Indeed, a structural alignment confirms that the G2 and G2F Fcs are almost identical with a main chain atom root square deviation (RMSD) of 0.59 Å for the monomers A and B that assemble to form the Fc dimer (Fig. 6A and B). In both structures, glycosyl groups attached to N297 were clearly visible permitting identification of the differences in sugar composition. As shown in Fig. 6C, the N297 sugar of both variants consists of a core formed by two *N*-acetyl-D-glucosamines (with the first attached directly to N297) and one β-D-mannose with two branching arms, an α(1-3) arm (α3 arm) linked to the O3 of the mannose and an α(1-6) arm (α6 arm) linked to the O6. Both arms consist of an α-D-mannose followed by *N*-acetyl-D-glucosamine. In addition, a terminal β-D-galactose is visible on the α6 arm (Fig. 6C, colored in cyan); a corresponding terminal galactose on the α3 arm, if present, is not visible due to disorder. The only major difference between the G2 and G2F forms is the lack of fucosyl group in afucosylated G2. The fucosyl group branches

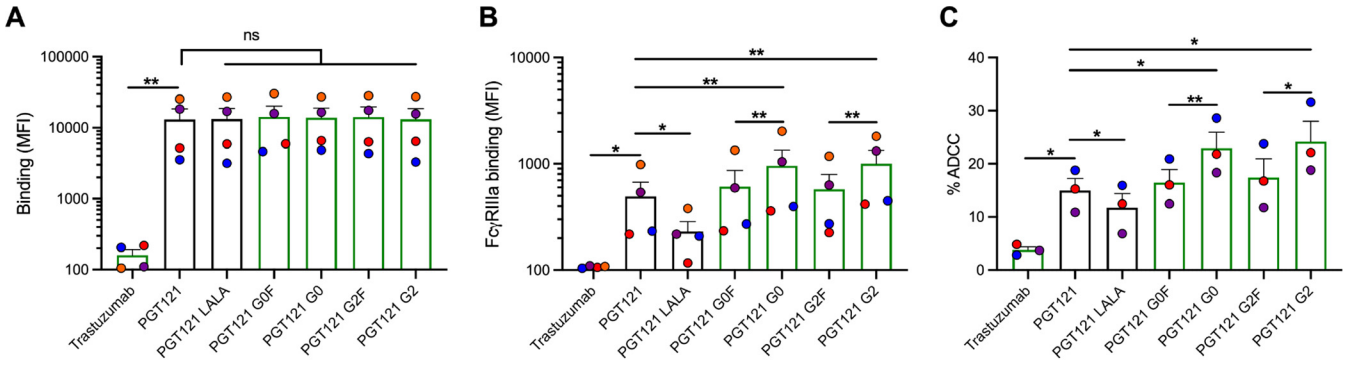

FIG 5 Susceptibility of *ex vivo*-expanded endogenously infected primary $CD4^+$ T cells from HIV-1-infected individuals to PGT121-mediated ADCC. Primary $CD4^+$ T cells from four different HIV-1-infected individuals were isolated and reactivated with PHA-L for 48 h, followed by incubation with IL-2 to expand the endogenous virus. Cell surface staining of infected primary $CD4^+$ T cells was performed upon reactivation. Antibody binding was detected either by using Alexa Fluor 647-conjugated anti-human secondary Abs (A) or biotin-tagged dimeric rsFcγRIIIa (0.2 μg/ml) followed by the addition of Alexa Fluor 647-conjugated streptavidin (B). (A and B) Graphs represent the MFI values in the infected population (p24+ or p27+) determined from at four different donors, with the error bars indicating means ± the SEM. (C) *Ex vivo*-expanded infected primary $CD4^+$ T cells from three HIV-1-infected individuals were used as target cells. Autologous PBMCs were used as effector cells in a FACS-based ADCC assay. The graphs represent the percentages of ADCC obtained in the presence of the respective antibodies. ADCC susceptibility was only measured when the percentage of infection (p24+ cells) was higher than 10%. Statistical significance was tested using a paired *t* test or Wilcoxon matched-pairs signed-rank test based on statistical normality (*, $P < 0.05$; **, $P < 0.01$; ***, $P < 0.001$; ns, nonsignificant). Black histogram bars represent 293F cell-derived MAbs, and green histogram bars represent plant-derived MAbs.

TABLE 2 Data collection and refinement statistics for fucosylated and afucosylated human Fc from *N. benthamiana*[a]

Parameter	Fucosylated human Fc	Afucosylated human Fc
Data collection		
Wavelength (Å)	0.920	0.979
Space group	$P2_12_12_1$	$P2_12_12_1$
Cell parameters		
a, *b*, *c* (Å)	49.9, 79.9, 138.5	49.7, 80.3, 137.0
α, β, γ (°)	90, 90, 90	90, 90, 90
Fcs/a.u.	1	1
Resolution (Å)	50–2.1 (2.21–2.1)	50–2.6 (2.74–2.6)
No. of reflections		
Total	106,578	54,596
Unique	32,561	15,294
R_{merge}[b] (%)	9.7 (77.5)	8.3 (90.2)
R_{pim}[c] (%)	6.1 (47.9)	4.7 (49.7)
$CC_{1/2}$[d]	0.99 (0.50)	0.99 (0.68)
I/σ	5.4 (1.0)	8.3 (1.8)
Completeness (%)	98.7 (99.3)	88.0 (90.2)
Redundancy	3.3 (3.4)	3.6 (3.6)
Refinement statistics		
Resolution (Å)	50.0–2.1	50.0–2.6
R[e] (%)	20.8	22.1
R_{free}[f] (%)	25.0	27.6
No. of atoms		
Protein	3,359	3,335
Water	189	20
Ligand/glycan	236	200
Overall B value (Å)^2		
Protein	59	81
Water	48	46
Ligand/ion	80	102
RMSD[g]		
Bond lengths (Å)	0.010	0.014
Bond angles (°)	1.1	1.6
Ramachandran (%)[h]		
Favored	96.6	90.3
Allowed	2.9	5.8
Outliers	0.5	3.9
PDB ID	6VSL	6VSZ

[a]Values in parentheses are for highest-resolution shell.
[b]$R_{merge} = \sum|I - \langle I\rangle|/\sum I$, where I is the observed intensity and is the average intensity obtained from multiple observations of symmetry-related reflections after rejections.
[c]R_{pim} = as defined by Weiss (88).
[d]$CC_{1/2}$ is as defined by Karplus and Diederichs (89).
[e]$R = \sum||F_o|-|F_c||/\sum|F_o|$, where F_o and F_c are the observed and calculated structure factors, respectively.
[f]R_{free} = as defined by Brünger (90).
[g]RMSD, root mean square deviation.
[h]Calculated with MolProbity.

directly off the first *N*-acetyl-D-glucosamine in the core attached to N297 in the G2F variant (Fig. 6C, colored in green). Of note, although the density for the Fc glycan attached to monomers A and B is visible in both the G2 and G2F structures, in both cases better quality density is observed for chain A. Chain B makes fewer crystal contacts resulting in more movement and higher b-factors for the chain B C_H2 domain and its attached glycan.

The C_H2-C_H3 homodimer is stabilized by interactions between the two C_H3 domains in the dimer, which are largely identical in both Fc variants (Fig. 6A and B). The glycans of opposing C_H2 domains are in close proximity but make no defined contacts to one another. The core β-D-mannose and the α6 arm of the glycan are stabilized by phenylalanines 241 and 243 of the C_H2 domain while the α3 arm is only stabilized by the opposing glycan in the dimer (Fig. 6D). The α6 arm is also stabilized by a hydrogen bond to lysine 246. This added stability facilitates the resolution of a terminal β-D-galactose which is in turn stabilized

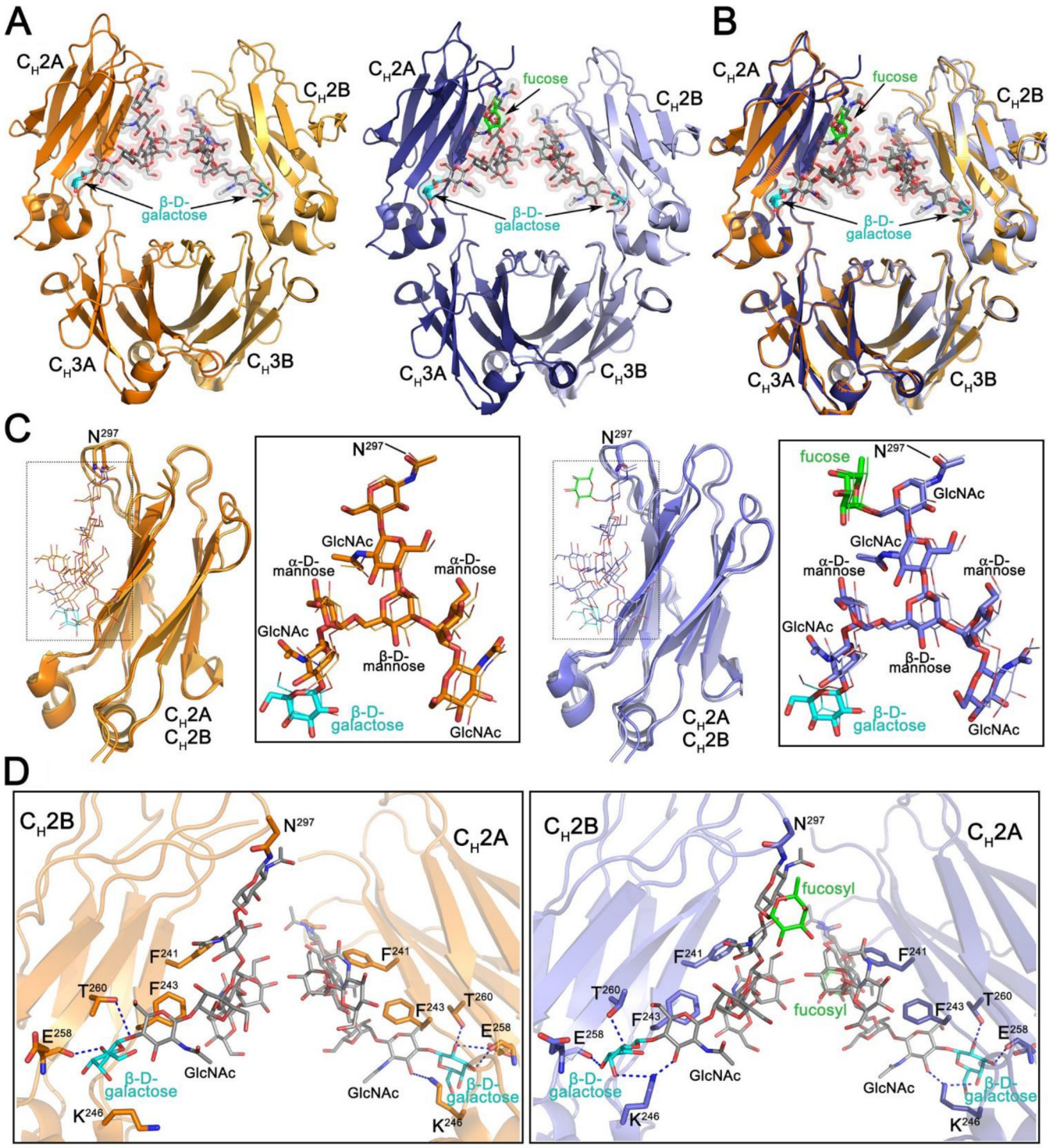

FIG 6 Structural characterization of the Fc regions of *N. benthamiana*-produced PGT121. (A) Crystal structures of afucosylated (right) and fucosylated (left) Fc. The overall structure is shown in a ribbon diagram with the two heavy chains (C_H2-C_H3 domains) in lighter (chain B) and darker (chain A) shades of orange and blue for afucosylated and fucosylated variants, respectively. The sugars attached to asparagine 297 are shown as sticks and spheres colored by atom type (gray for carbon, red for oxygen, and blue for nitrogen). The fucose in the fucosylated Fc is colored green and the terminal galactose visible on the α6 arm of the glycan in both structures cyan. (B) Superposition of the afucosylated and fucosylated C_H2-C_H3 dimer (Fc domain) colored as in panel A. (C) Superposition of the C_H2 domains from the afucosylated (left) and fucosylated (right) Fc dimer. Blow-up views to the right show the superposition of the glycan only with chain A shown as sticks and chain B as lines. Atom types are colored as in panel A. (D) Details of the glycan-glycan and glycan-protein contacts in the afucosylated (left) and fucosylated (right) Fc dimers. The glycan and interacting residues are shown as sticks and the protein backbone as a ribbon. Hydrogen bonds are shown with dashed lines. Atom types are colored as in panel A.

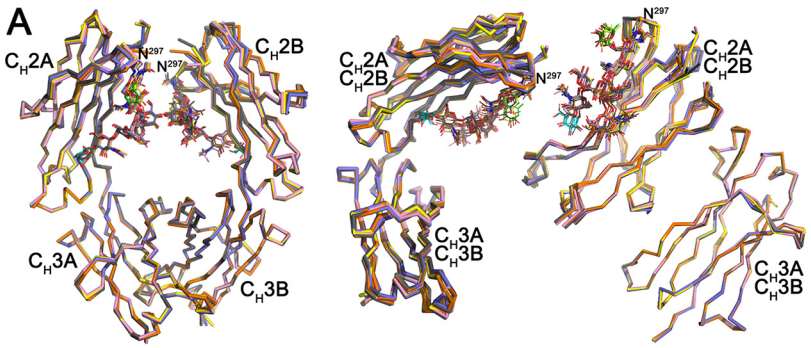

B

C_H2 domain

C_H3 domain						C_H2 domain
3AVE	3AVE	1.09	1.23	1.37	1.17	
2DTS	0.87	2DTS	1.28	1.43	1.30	
5VGP	0.87	0.90	5VGP	1.45	1.16	
afucosyl.	0.85	0.99	0.93	afucosyl.	1.33	
fucosyl.	0.75	0.93	0.82	0.78	fucosyl.	

C_H3 domain

C_H2-C_H3 dimer (Fc domain)

C_H2-C_H3 monomer						C_H2-C_H3 dimer (Fc domain)
3AVE	3AVE	0.41	0.53	0.63	0.56	
2DTS	0.65	2DTS	0.67	0.69	0.67	
5VGP	0.84	0.87	5VGP	0.63	0.39	
afucosyl.	0.84	0.82	0.91	afucosyl.	0.59	
fucosyl.	0.85	0.86	0.84	0.87	fucosyl.	

C_H2-C_H3 monomer

FIG 7 Comparison of the overall structures of *N. benthamiana* expressed and mammalian expressed human Fc domains. Structural alignment of C_H2-C_H3 dimers (Fc), C_H2-C_H3 monomers, C_H2 domains, and C_H3 domains of *N. benthamiana* and mammalian expressed human Fcs including the following: a human fucosylated Fc lacking the terminal galactose (PDB ID 3AVE, yellow), an afucosylated Fc (2DTS, pink), and a fucosylated Fc containing a terminal galactose (5VGP, gray). *N. benthamiana* expressed Fcs are colored as in Fig. 6, with fucose colored green and galactose cyan. (B) Average RMSD values for main chain atom pairwise comparisons of C_H2 domains, C_H3 domains, C_H2-C_H3 monomers, and C_H2-C_H3 dimers (Fc domain) shown in tabular format color coded with smaller RMSD values green and larger RMSD values red.

by hydrogen bonds to the carbonyl oxygen of glutamate 258 and the side chain of threonine 260. Details of the α3 arm past the *N*-acetyl-D-glucosamine are not seen due to movement in the crystal.

The structures presented in Fig. 6 allowed us to compare our plant-derived G2 and G2F PGT121 Fc structures with previously published structures of mammalian cell-expressed Fc domains: a fucosylated Fc lacking the terminal galactose (G0F) (PDB ID 3AVE), an afucosylated Fc (G0) (PDB ID 2DTS), and a fucosylated Fc containing a terminal galactose (G2F) (PDB ID 5VGP). As shown in Fig. 7A, where the structures of the Fc dimer, the C_H2-C_H3 monomer and the individual CH_2 and CH_3 domains are overlaid, there is very close similarity between equivalent fucosylated and afucosylated variants of plant and mammalian derived Fcs. Figure 7B summarizes the root mean square deviation (RMSD) values for all comparisons, which show that the C_H3 domain is the most structurally similar among the comparisons with RMSDs less than 1 Å. Bigger differences are seen for the both the plant and mammalian expressed afucosylated structures. The same holds true for the comparison of the C_H2 domains but the magnitude of the RMSD is higher, 1.1 to 1.5 Å, reflecting the influence of the glycan bound to N297. Looking at the Fc as a whole, a similar pattern emerges with a greater range of RMSD variation for the afucosylated compared to the fucosylated Fc. This greater variability is more apparent in the dimer than the monomer, supporting the interpretation that these differences are a consequence of glycan composition. However, given these differences, both plant and mammalian expressed Fc domains are largely identical with respect to expression origin.

DISCUSSION

The results presented in this study suggest that *N. benthamiana* can be used as a reliable platform to produce bNAbs targeting HIV-1. No overall differences in viral neutralization and binding of Env but enhanced FcγRIIIa engagement and ADCC against infected cells were observed with some of the plant-derived PGT121 MAbs compared to the 293F-produced PGT121. Importantly, Fc structures were found to be nearly identical whether the MAbs were produced in plants or in mammalian cell lines. The safety of plant-produced biological therapeutics and the value of having a rapid and adaptable system for MAb production was demonstrated during the 2014-2016 Ebolavirus (EBOV) outbreak in West Africa (64). ZMapp, a cocktail of MAbs targeting the EBOV envelope glycoprotein, was produced in *N. benthamiana* bearing predominantly G0 glycans and was used as a therapeutic treatment for EBOV disease (65). No major safety concerns were observed, while individuals receiving the ZMapp had reduced mortality, as well as significantly shorter stays in treatment units (64).

Another advantage of using the *N. benthamiana* system is the ability to engineer the N-linked glycan composition of MAbs present on the Fc region of antibodies, which critically affects their affinity for FcγRs. Furthermore, using the KDFX transgenic *N. benthamiana* system, Fc regions of IgG proteins are systematically glycosylated with the G0 glycoform, without any core fucose or terminal galactose moieties (18, 66). The role of core fucosylation has been shown to be a strong determinant in the Fc affinity for FcγRIIIa and the removal of the fucose from the IgG Fc increases its affinity to FcγRIIIa (60, 67). Consequently, afucosylated MAbs can mediate significantly stronger ADCC responses (28, 67). Our results of improved FcγRIIIa interaction and ADCC activities of afucosylated PGT121 against SHIV- or HIV-1-infected cells, as well as endogenously HIV-1-infected cells, cumulatively suggests that the MAb glycosylation profile can dictate its Fc-mediated effector functionality.

The presence of galactose has also been shown to enhance FcγRIIIa binding (68). However, there exists conflicting evidence on the role of galactosylation on antibody functionality. Some studies have found only modest differences between the presence or absence of galactose on Ab *in vivo* activities (69, 70). When considering the galactosylation status of PGT121 (G0 or G2), we observed a slight enhancement of ADCC mediated by galactosylated PGT121 against CEM.NKr cells infected with HIV-1_{JRCSF}. However, no significant differences were seen in a more physiologically relevant context, i.e., against primary $CD4^+$ T cells. We believe these differences could be due to the lower cell surface level of Env present on CEM.NKr cells, which could impact ADCC responses (71). Furthermore, as the observation by recent studies that the absence of fucose is more predominant than the presence of galactose on the ADCC activity of therapeutic MAbs (72), our results also strongly suggest that N-linked galactosylation is not required for the improved functionality of afucosylated PGT121. Lastly, to translationally utilize the *N. benthamiana* system to produce bNAbs targeting HIV-1, it is important to ensure high N-glycan homogeneity (51).

PGT121 was recently used in combination with a TLR7 agonist as an attempt to eliminate the cellular reservoir in SHIV-infected macaques (73, 74). PGT121 is also currently being tested in combination with other bNAbs for HIV-1 prophylaxis and therapy in clinical trials (NCT03721510). Two recent studies showed that the neutralization capacity of PGT121 is sufficient to protect NHP from SHIV challenges (42, 43). In these studies, Fc-impaired versions of PGT121 provided similar levels of protection as their wild-type counterparts. However, these studies were performed with primarily fucosylated PGT121 and did not comprehensively explore the capacity of PGT121 to clear the cellular reservoir. Passive administration of other potent bNAbs have been shown to decrease the number of infected cells and suppress viremia in animal models and infected individuals (2, 9, 12), with important contributions from their Fc-mediated effector functions (45). Our results suggest that afucosylated PGT121 could boost its Fc-mediated effector capacity and thus its antiviral activity when used with a focus of controlling existing infection and decreasing disease progression.

MATERIALS AND METHODS

Ethics statement. Written informed consent was obtained from all study participants in the Montreal Primary HIV Infection Cohort (75, 76), and research adhered to the ethical guidelines of

CRCHUM and was reviewed and approved by the CRCHUM institutional review board (ethics committee, approval number CE16.164-CA). Research adhered to the standards indicated by the Declaration of Helsinki. All participants were adult and provided informed written consent prior to enrollment in accordance with Institutional Review Board approval.

Cell lines and isolation of primary CD4$^+$ T cells. 293T human embryonic kidney cells (obtained from ATCC) were maintained at 37°C under 5% CO_2 in Dulbecco modified Eagle medium (Wisent) containing 5% fetal bovine serum (VWR) and 100 μg/ml penicillin-streptomycin (Wisent). CEM.NKR-CCR5-sLTR-Luc cells and the CD16$^+$ KHYG-1 effector cells were maintained at 37°C under 5% CO_2 in RPMI 1640 complete medium (Gibco) containing 10% fetal bovine serum (VWR) and 100 μg/ml penicillin-streptomycin (Wisent). Primary CD4$^+$ T lymphocytes were purified from resting PBMCs by negative selection and activated as previously described (56, 71). Briefly, PBMCs were obtained by leukapheresis from 5 HIV-uninfected healthy adults. CD4$^+$ T lymphocytes were purified using immunomagnetic beads as per the manufacturer's instructions (Stem Cell Technologies). CD4$^+$ T lymphocytes were activated with phytohemagglutinin-L (PHA-L; 10 μg/ml) for 48 h and then maintained in RPMI 1640 complete medium (Gibco) supplemented with rIL-2 (100 U/ml).

Plant-derived protein production and purification. Methods for production of antibodies in plants have been published (18, 21, 77, 78). Expression vectors for plant-produced trastuzumab and PGT121 were assembled in a common plasmid backbone and included a double-enhancer version of the Cauliflower Mosaic Virus 35S promoter (EE35S) (79) driving expression of each of the respective heavy-chain and light-chain genes plus the same promoter driving expression of Tomato Bushy Stunt Virus P19 protein (22). A P19-only expression vector, assembled in similar fashion, was also used in some plant treatments. Posttranslational modification vectors were also assembled similarly: oligosaccharidyltransferase STT3D (80), driven by the *Arabidopsis* Act2 promoter (81); alpha-mannosidase GMII from *N. benthamiana* (Niben101Scf06280g02001.1; solgenomics.net), driven by the EE35S or Act2 promoters; *N*-acetylglucosaminyltransferase GnTII from *N. benthamiana* (Niben101Scf16329g00007.1; solgenomics.net), driven by the EE35S or Act2 promoters; human β-1,4-galactosyltransferase (GalT [82]), driven by the basal 35S promoter; and human α-1,6-fucosyltransferase (FucT; NCBI reference sequence NP_835368.1), driven by the Act2 promoter. All plant-produced antibody and glycomodification enzyme coding sequences were designed to incorporate preferred *N. benthamiana* codons according to published methods (83, 84). Antibodies were purified using protein A (HiTrap MabSelect) and polished with Capto Q (HiTrap Capto Q) columns according to manufacturer protocols (Cytiva Life Sceinces, Chicago, IL). Purified antibodies were dialyzed against PBS. To assess purity, SDS-PAGE and immunoblotting were performed according to published methods (78). Galactosylated and fucosylated antibodies were confirmed via immunoblotting with biotinylated *Ricinus communis* agglutinin I for galactose or biotinylated *Aleuria aurantia* lectin for fucose (both lectins were from Vector Labs), followed by horseradish peroxidase-conjugated streptavidin (BioLegend) and chemiluminescent signal development with SuperSignal West Pico Chemiluminescent Substrate (Thermo Fisher) (data not shown). Glycan analyses were as described previously (21). Briefly, glycans were prepared using a GlykoPrep Rapid N-Glycan preparation kit (PROzyme, Hawyard, CA) and separated by hydrophilic-interaction liquid chromatography using a TSKgel Amide-80 column (Tosoh Bioscience, Grove City, OH) and then identified by relative retention time and quantified using autointegration of glycan peaks. Crystallizable fragments (Fcs) of *N. benthamiana*-expressed afucosylated and fucosylated PGT121 IgG were generated by papain digest. Digested Fab and Fc were separated by protein A affinity purification on a HiTrap protein A affinity column (GE Healthcare, Piscataway, NJ) equilibrated in phosphate-buffered saline (PBS). The Fc fragment was eluted with 0.1 M glycine (pH 3.0), and the pH of the eluted fractions was increased by the addition of 1 M Tris-HCl (pH 8.5). Fc was separated from undigested IgG by gel filtration chromatography on a Superdex 200 16/60 column (GE Healthcare, Piscataway, NJ) equilibrated in 10 mM Tris-HCl (pH 7.2) and 0.1 M ammonium acetate. Elution fractions corresponding to the predicted Fc molecular weight were combined and concentrated to ~10 mg/ml for crystallization experiments.

Mammalian cell-derived protein production and purification. PGT121 and PGT121 LALA antibodies produced in 293F cells were acquired from Scripps Research Institute Antibody Core Facility (La Jolla, CA). FreeStyle 293F cells (Thermo Fisher Scientific) were grown in FreeStyle 293F medium (Thermo Fisher Scientific) to a density of 1×10^6 cells/ml at 37°C with 8% CO_2 with regular agitation (150 rpm). Cells were transfected with a plasmid expressing the dimeric recombinant soluble FcγRIIIa V^{158} (rsFcγRIIIa) (61) using ExpiFectamine 293 transfection reagent, as directed by the manufacturer (Thermo Fisher Scientific). 1 week later, the cells were pelleted, and supernatants were filtered using a 0.22-μm-pore-size filter (Thermo Fisher Scientific). The rsFcγRIIIa proteins were purified by nickel affinity columns, as directed by the manufacturer (Thermo Fisher Scientific). Furthermore, the purified rsFcγRIIIa proteins were biotinylated using the EZ-Link Sulfo-NHS-LC-Biotinylation kit according to the manufacturer's instructions (Themo Fisher Scientific).

X-ray crystallography, structure solution, and refinement. Crystals of both Fc isoforms were grown by the hanging drop vapor diffusion method from 15% PEG 4000 and 0.1 M HEPES (pH 7.0). Data were collected on crystals that had been flash frozen in liquid nitrogen. To prevent ice formation upon freezing, crystals were briefly soaked in crystallization buffer with 20% 2-methyl-2,4-pentanediol (MPD) added as a cryoprotectant. Data were collected on the National Synchrotron Light Source II (NSLS II) Highly Automated Macromolecular Crystallography (AMX) beam line (17-ID-1). Data were integrated and scaled with mosflm and scala from the CCP4 suite of programs. Structures were solved by molecular replacement with Phaser from the CCP4 suite based on the coordinates of 3AVE (a human fucosylated Fc). Refinement was carried out with Refmac and/or Phenix and model building was done with COOT. Data collection and refinement statistics are shown in Table 2. Ramachandran statistics were calculated with Molprobity and illustrations were prepared with PyMOL Molecular graphics (http://pymol.org). The b-factor, also called a temperature factor or atomic displacement parameter, indicates the precision of the atom positions in the crystallographic structures on

macromolecules. A higher b-factor corresponds to the increased movement (disorder) of the given atom. Atom positions can be uncertain because of disorder in the crystal from which the structure was determined.

Viral production, infections, and *ex vivo* amplification. For *in vitro* infection, vesicular stomatitis virus G (VSV-G)-pseudotyped HIV-1_{JRCSF} (NIH AIDS Reagent Program), $SHIV_{AD8\text{-}EO}$ (kindly provided by Malcom Martin), and $SHIV_{BG505}$ IMCs were produced in 293T cells and titrated as previously described (56). The $SHIV_{BG505}$ IMC harbors the T332N and S375Y mutations in its Env (85). Viruses were then used to infect CEM.NKr CCR5$^+$ cells or primary CD4 T cells from healthy donors by spin infection at 800 $\times$ *g* for 1 h in 96-well plates at 25°C. To expand endogenously infected CD4$^+$ T cells, primary CD4$^+$ T cells obtained from four ART-treated HIV-1-infected individuals were isolated from PBMCs by negative selection. Purified CD4$^+$ T cells were activated with PHA-L at 10 μg/ml for 48 h and then cultured for at least 6 days in RPMI 1640 complete medium supplemented with rIL-2 (100 U/ml) to reach greater than 10% infection for the ADCC assay. ADCC susceptibility was not assessed for one of the donors since it only reached 4% infection.

Flow cytometry analysis of cell surface staining. Cell surface staining of infected cells was performed as previously described (55, 63, 86). Binding to cell surface HIV-1 Env by anti-Env MAbs (5 μg/ml) was performed at 48 h postinfection. Goat anti-human Alexa Fluor 647 secondary Abs (Thermo Fisher Scientific) was used to determine overall antibody binding and AquaVivid (Thermo Fisher Scientific) as a viability dye. Alexa Fluor 647-conjugated streptavidin (Thermo Fisher Scientific) was used to determine biotin-tagged dimeric recombinant soluble FcγRIIIa (V^{158}) binding. Cells were then permeabilized using a Cytofix/Cytoperm fixation/permeabilization kit (BD Biosciences). HIV-1-infected cells were identified by intracellular staining of p24 using phycoerythrin-conjugated anti-p24 MAb (clone KC57; Beckman Coulter) and SHIV-infected cells were identified by intracellular staining using Alexa Fluor 488-conjugated anti-p27 Abs (clone 2F12). The percentage of infected cells (p24+ or p27+ cells) was determined by gating the living cell population based on viability dye staining with AquaVivid (Thermo Fisher Scientific). Samples were analyzed on a Fortessa cytometer (BD Biosciences), and data analysis was performed using FlowJo v10.7.1 (Tree Star).

FACS-based ADCC assay. Measurement of ADCC using the FACS-based assay was performed at 48 h postinfection as previously described (55, 63, 87) or after reaching 10% of p24+ cells during *ex vivo* expansion. Briefly, infected cells were stained with AquaVivid viability dye and cell proliferation dye (eFluor670; eBioscience) and used as target cells. Autologous PBMCs were used as effectors cells and were stained with another cellular dye (cell proliferation dye eFluor450; eBioscience). Effector and target cells were mixed at a ratio of 10:1 in 96-well V-bottom plates (Corning), and 5 μg/ml of MAbs was added to appropriate wells. The plates were subsequently centrifuged for 1 min at 300 $\times$ *g* and incubated at 37°C and 5% CO_2 for 5 h before being fixed in a 2% PBS-formaldehyde solution. Samples were acquired on a Fortessa cytometer (BD Biosciences), and data analysis was performed using FlowJo v10.7.1 (Tree Star). The percentage of ADCC was calculated using the following formula: (% of p24+ or p27+ cells in targets plus effectors) − (% of p24+ or p27+ cells in targets plus effectors plus Abs)/(% of p24+ or p27+ cells in targets) by gating on live target cells.

Luciferase-based ADCC assay. Measurement of ADCC responses using the luciferase reporter assay was performed as previously described with a NK cell line stably expressing human CD16a serving as effector cells (44, 57–59). The lymphocytic cell line CEM.NKR-CCR5-sLTR-Luc, which expresses the firefly luciferase (Luc) under the control of a Tat-inducible promoter, was infected with VSV G-pseudotyped $SHIV_{AD8\text{-}EO}$ and used as target cells. To avoid VSV G-pseudotyping replication-competent virus, a 2-bp deletion was introduced into the *vif* gene of $SHIV_{AD8\text{-}EO}$, resulting in a premature stop codon followed by a frameshift. At 2 days postinfection, effector cells were incubated with target cells for 8 h, in triplicate, at a ratio of 10:1 in the presence of different concentrations of Abs ranging from 100 μg/ml to 0.006 μg/ml using a 4-fold dilution factor. The dose-dependent loss of Luc activity was measured as an indication of Ab-mediated killing of productively infected cells. Infected target cells incubated with effector cells in the absence of Ab were used to measure maximal Luc activity, and uninfected target cells cultured with effector cells were used to determine background Luc activity. ADCC activity as a percentage of relative light units (RLU) was calculated as follows: (mean RLU at a given antibody concentration − mean background RLU)/(mean maximal RLU − mean background RLU) $\times$ 100. Area under the curve (AUC) values for ADCC were calculated from the percent RLU, as previously described (44, 57–59).

Virus neutralization. Lentiviral particles were produced in HEK 293T using the standard calcium phosphate transfection technique. Two days posttransfection, cell supernatants were harvested. TZM-bl target cells were seeded at a density of 1×10^4 cells/well in 96-well luminometer-compatible tissue culture plates (Perkin-Elmer) 24 h before infection. Viral preparations were incubated for 1 h at 37°C with serial dilutions of anti-Env antibodies in a final volume of 200 μl before being added to the target cells. After a 48-h incubation at 37°C, the medium was removed from each well, and cells were lysed by the addition of 30 μl of passive lysis buffer (Promega), followed by one freeze-thaw cycle. An LB941 TriStar luminometer (Berthold Technologies) was used to measure the luciferase activity of each well after the addition of 100 μl of luciferin buffer (15 mM $MgSO_4$, 15 mM KPO_4 [pH 7.8], 1 mM ATP, and 1 mM dithiothreitol) and 50 μl of 1 mM D-luciferin potassium salt (Prolume).

Statistical analyses. Statistics were analyzed using Prism version 9.0.0 (GraphPad, San Diego, CA). Every data set was tested for statistical normality using the Shapiro-Wilk test, and this information was used to apply the appropriate (parametric or nonparametric) statistical test. *P* values of <0.05 were considered significant; significance values are indicated in the figures by asterisks (*, $P < 0.05$; **, $P < 0.01$; ***, $P < 0.001$; ****, $P < 0.0001$).

Data availability. Fucosylated and afucosylated Fc structures were deposited in the Protein Data Bank (PDB) with PDB IDs 6VSL and 6VSZ, respectively.

ACKNOWLEDGMENTS

We thank the CRCHUM Flow Cytometry and Biosafety Level 3 Laboratory Platforms and Mario Legault for cohort coordination and clinical samples.

This study was supported by a National Research Council (Canada) Industrial Research Assistance Program (NRC-IRAP) grant to M.D.M. and A.F., by CIHR foundation grant 352417 to A.F., and by NIH grants R01 AI129 AI129769 to M.P. and A.F., R01 AI116274 to M.P., P01 AI120756 to Georgia Tomaras, R01 AI121135 and R37 AI095098 to D.T.E., and R01 AI148379 to A.F. and D.T.E. A.F. is the recipient of a Canada Research Chair on Retroviral Entry (grant RCHS0235 950-232424). L.H. was supported by NIH R01 AI136621-02 and NIH UM1 AI144462-01. D.R.B. was supported by NIH UM1 AI144462. Plant antibody production and analyses by PlantForm Corporation were supported in part by NRC-IRAP (catalog no. 778829 and 812182), and glycosylation analyses were performed by Warren Wakarchuk. S.P.A. and J.P. are supported by CIHR fellowships. This research used resources of the National Synchrotron Light Source II, a U.S. Department of Energy (DOE) Office of Science User Facility operated for the DOE Office of Science by the Brookhaven National Laboratory under contract DE-SC0012704. The Center for BioMolecular Structure (CBMS) is primarily supported by the National Institutes of Health, National Institute of General Medical Sciences (NIGMS), through a Center Core P30 grant (P30GM133893) and by the DOE Office of Biological and Environmental Research (KP1607011). The funders had no role in study design, data collection and analysis, the decision to publish, or preparation of the manuscript.

W.F.C., H.W., R.P., D.C., and M.D.M. are all employees of PlantForm Corporation.

The views expressed in this presentation are those of the authors and do not reflect the official policy or position of the Uniformed Services University, the U.S. Army, the Department of Defense, or the U.S. Government.

REFERENCES

1. Barouch DH, Whitney JB, Moldt B, Klein F, Oliveira TY, Liu J, Stephenson KE, Chang HW, Shekhar K, Gupta S, Nkolola JP, Seaman MS, Smith KM, Borducchi EN, Cabral C, Smith JY, Blackmore S, Sanisetty S, Perry JR, Beck M, Lewis MG, Rinaldi W, Chakraborty AK, Poignard P, Nussenzweig MC, Burton DR. 2013. Therapeutic efficacy of potent neutralizing HIV-1-specific monoclonal antibodies in SHIV-infected rhesus monkeys. Nature 503:224–228. https://doi.org/10.1038/nature12744.
2. Bournazos S, Klein F, Pietzsch J, Seaman MS, Nussenzweig MC, Ravetch JV. 2014. Broadly neutralizing anti-HIV-1 antibodies require Fc effector functions for *in vivo* activity. Cell 158:1243–1253. https://doi.org/10.1016/j.cell.2014.08.023.
3. Horwitz JA, Halper-Stromberg A, Mouquet H, Gitlin AD, Tretiakova A, Eisenreich TR, Malbec M, Gravemann S, Billerbeck E, Dorner M, Buning H, Schwartz O, Knops E, Kaiser R, Seaman MS, Wilson JM, Rice CM, Ploss A, Bjorkman PJ, Klein F, Nussenzweig MC. 2013. HIV-1 suppression and durable control by combining single broadly neutralizing antibodies and antiretroviral drugs in humanized mice. Proc Natl Acad Sci U S A 110:16538–-16543. https://doi.org/10.1073/pnas.1315295110.
4. Klein F, Halper-Stromberg A, Horwitz JA, Gruell H, Scheid JF, Bournazos S, Mouquet H, Spatz LA, Diskin R, Abadir A, Zang T, Dorner M, Billerbeck E, Labitt RN, Gaebler C, Marcovecchio P, Incesu RB, Eisenreich TR, Bieniasz PD, Seaman MS, Bjorkman PJ, Ravetch JV, Ploss A, Nussenzweig MC. 2012. HIV therapy by a combination of broadly neutralizing antibodies in humanized mice. Nature 492:118–122. https://doi.org/10.1038/nature11604.
5. Hessell AJ, Poignard P, Hunter M, Hangartner L, Tehrani DM, Bleeker WK, Parren PW, Marx PA, Burton DR. 2009. Effective, low-titer antibody protection against low-dose repeated mucosal SHIV challenge in macaques. Nat Med 15:951–954. https://doi.org/10.1038/nm.1974.
6. Hessell AJ, Rakasz EG, Poignard P, Hangartner L, Landucci G, Forthal DN, Koff WC, Watkins DI, Burton DR. 2009. Broadly neutralizing human anti-HIV antibody 2G12 is effective in protection against mucosal SHIV challenge even at low serum neutralizing titers. PLoS Pathog 5:e1000433. https://doi.org/10.1371/journal.ppat.1000433.
7. Hessell AJ, Rakasz EG, Tehrani DM, Huber M, Weisgrau KL, Landucci G, Forthal DN, Koff WC, Poignard P, Watkins DI, Burton DR. 2010. Broadly neutralizing monoclonal antibodies 2F5 and 4E10 directed against the human immunodeficiency virus type 1 gp41 membrane-proximal external region protect against mucosal challenge by simian-human immunodeficiency virus SHIVBa-L. J Virol 84:1302–1313. https://doi.org/10.1128/JVI.01272-09.
8. Caskey M, Klein F, Lorenzi JC, Seaman MS, West AP, Jr, Buckley N, Kremer G, Nogueira L, Braunschweig M, Scheid JF, Horwitz JA, Shimeliovich I, Ben-Avraham S, Witmer-Pack M, Platten M, Lehmann C, Burke LA, Hawthorne T, Gorelick RJ, Walker BD, Keler T, Gulick RM, Fatkenheuer G, Schlesinger SJ, Nussenzweig MC. 2015. Viraemia suppressed in HIV-1-infected humans by broadly neutralizing antibody 3BNC117. Nature 522:487–491. https://doi.org/10.1038/nature14411.
9. Caskey M, Schoofs T, Gruell H, Settler A, Karagounis T, Kreider EF, Murrell B, Pfeifer N, Nogueira L, Oliveira TY, Learn GH, Cohen YZ, Lehmann C, Gillor D, Shimeliovich I, Unson-O'Brien C, Weiland D, Robles A, Kummerle T, Wyen C, Levin R, Witmer-Pack M, Eren K, Ignacio C, Kiss S, West AP, Jr, Mouquet H, Zingman BS, Gulick RM, Keler T, Bjorkman PJ, Seaman MS, Hahn BH, Fatkenheuer G, Schlesinger SJ, Nussenzweig MC, Klein F. 2017. Antibody 10-1074 suppresses viremia in HIV-1-infected individuals. Nat Med 23:185–191. https://doi.org/10.1038/nm.4268.
10. Lynch RM, Boritz E, Coates EE, DeZure A, Madden P, Costner P, Enama ME, Plummer S, Holman L, Hendel CS, Gordon I, Casazza J, Conan-Cibotti M, Migueles SA, Tressler R, Bailer RT, McDermott A, Narpala S, O'Dell S, Wolf G, Lifson JD, Freemire BA, Gorelick RJ, Pandey JP, Mohan S, Chomont N, Fromentin R, Chun T-W, Fauci AS, Schwartz RM, Koup RA, Douek DC, Hu Z, Capparelli E, Graham BS, Mascola JR, Ledgerwood JE, Team VRCS. 2015. Virologic effects of broadly neutralizing antibody VRC01 administration during chronic HIV-1 infection. Sci Transl Med 7:319ra206. https://doi.org/10.1126/scitranslmed.aad5752.
11. Gautam R, Nishimura Y, Pegu A, Nason MC, Klein F, Gazumyan A, Golijanin J, Buckler-White A, Sadjadpour R, Wang K, Mankoff Z, Schmidt SD, Lifson JD, Mascola JR, Nussenzweig MC, Martin MA. 2016. A single injection of anti-HIV-1 antibodies protects against repeated SHIV challenges. Nature 533:105–109. https://doi.org/10.1038/nature17677.
12. Mendoza P, Gruell H, Nogueira L, Pai JA, Butler AL, Millard K, Lehmann C, Suarez I, Oliveira TY, Lorenzi JCC, Cohen YZ, Wyen C, Kummerle T, Karagounis T, Lu CL, Handl L, Unson-O'Brien C, Patel R, Ruping C, Schlotz M, Witmer-Pack M, Shimeliovich I, Kremer G, Thomas E, Seaton KE, Horowitz J, West AP, Jr, Bjorkman PJ, Tomaras GD, Gulick RM, Pfeifer N, Fatkenheuer G, Seaman MS, Klein F, Caskey M, Nussenzweig MC. 2018. Combination therapy with anti-HIV-1 antibodies maintains viral suppression. Nature 561:479–484. https://doi.org/10.1038/s41586-018-0531-2.
13. Ecker DM, Jones SD, Levine HL. 2015. The therapeutic monoclonal antibody market. MAbs 7:9–14. https://doi.org/10.4161/19420862.2015.989042.
14. Nandi S, Kwong AT, Holtz BR, Erwin RL, Marcel S, McDonald KA. 2016. Techno-economic analysis of a transient plant-based platform for monoclonal antibody production. MAbs 8:1456–1466. https://doi.org/10.1080/19420862.2016.1227901.

15. Robinson MP, Ke N, Lobstein J, Peterson C, Szkodny A, Mansell TJ, Tuckey C, Riggs PD, Colussi PA, Noren CJ, Taron CH, DeLisa MP, Berkmen M. 2015. Efficient expression of full-length antibodies in the cytoplasm of engineered bacteria. Nat Commun 6:8072. https://doi.org/10.1038/ncomms9072.
16. Potgieter TI, Cukan M, Drummond JE, Houston-Cummings NR, Jiang Y, Li F, Lynaugh H, Mallem M, McKelvey TW, Mitchell T, Nylen A, Rittenhour A, Stadheim TA, Zha D, d'Anjou M. 2009. Production of monoclonal antibodies by glycoengineered Pichia pastoris. J Biotechnol 139:318–325. https://doi.org/10.1016/j.jbiotec.2008.12.015.
17. Ma JK, Drossard J, Lewis D, Altmann F, Boyle J, Christou P, Cole T, Dale P, van Dolleweerd CJ, Isitt V, Katinger D, Lobedan M, Mertens H, Paul MJ, Rademacher T, Sack M, Hundleby PA, Stiegler G, Stoger E, Twyman RM, Vcelar B, Fischer R. 2015. Regulatory approval and a first-in-human phase I clinical trial of a monoclonal antibody produced in transgenic tobacco plants. Plant Biotechnol J 13:1106–1120. https://doi.org/10.1111/pbi.12416.
18. McLean MD. 2017. Trastuzumab made in plants using vivoXPRESS platform technology. J Drug Des Res 4:1052.
19. Tschofen M, Knopp D, Hood E, Stoger E. 2016. Plant molecular farming: much more than medicines. Annu Rev Anal Chem (Palo Alto Calif) 9:271–294. https://doi.org/10.1146/annurev-anchem-071015-041706.
20. Tuse D, Tu T, McDonald KA. 2014. Manufacturing economics of plant-made biologics: case studies in therapeutic and industrial enzymes. Biomed Res Int 2014:256135. https://doi.org/10.1155/2014/256135.
21. Park JG, Ye C, Piepenbrink MS, Nogales A, Wang H, Shuen M, Meyers AJ, Martinez-Sobrido L, Kobie JJ. 2020. A broad and potent H1-specific human monoclonal antibody produced in plants prevents influenza virus infection and transmission in guinea pigs. Viruses 12:167. https://doi.org/10.3390/v12020167.
22. Garabagi F, Gilbert E, Loos A, McLean MD, Hall JC. 2012. Utility of the P19 suppressor of gene-silencing protein for production of therapeutic antibodies in *Nicotiana* expression hosts. Plant Biotechnol J 10:1118–1128. https://doi.org/10.1111/j.1467-7652.2012.00742.x.
23. Strasser R, Altmann F, Steinkellner H. 2014. Controlled glycosylation of plant-produced recombinant proteins. Curr Opin Biotechnol 30:95–100. https://doi.org/10.1016/j.copbio.2014.06.008.
24. Diamos AG, Hunter JGL, Pardhe MD, Rosenthal SH, Sun H, Foster BC, DiPalma MP, Chen Q, Mason HS. 2019. High-level production of monoclonal antibodies using an optimized plant expression system. Front Bioeng Biotechnol 7:472. https://doi.org/10.3389/fbioe.2019.00472.
25. Dent M, Hurtado J, Paul AM, Sun H, Lai H, Yang M, Esqueda A, Bai F, Steinkellner H, Chen Q. 2016. Plant-produced anti-dengue virus monoclonal antibodies exhibit reduced antibody-dependent enhancement of infection activity. J Gen Virol 97:3280–3290. https://doi.org/10.1099/jgv.0.000635.
26. van Dolleweerd CJ, Teh AY, Banyard AC, Both L, Lotter-Stark HC, Tsekoa T, Phahladira B, Shumba W, Chakauya E, Sabeta CT, Gruber C, Fooks AR, Chikwamba RK, Ma JK. 2014. Engineering, expression in transgenic plants and characterization of E559, a rabies virus-neutralizing monoclonal antibody. J Infect Dis 210:200–208. https://doi.org/10.1093/infdis/jiu085.
27. He J, Lai H, Engle M, Gorlatov S, Gruber C, Steinkellner H, Diamond MS, Chen Q. 2014. Generation and analysis of novel plant-derived antibody-based therapeutic molecules against West Nile virus. PLoS One 9:e93541. https://doi.org/10.1371/journal.pone.0093541.
28. Shields RL, Lai J, Keck R, O'Connell LY, Hong K, Meng YG, Weikert SH, Presta LG. 2002. Lack of fucose on human IgG1 N-linked oligosaccharide improves binding to human Fcγ RIII and antibody-dependent cellular toxicity. J Biol Chem 277:26733–26740. https://doi.org/10.1074/jbc.M202069200.
29. Shields RL, Namenuk AK, Hong K, Meng YG, Rae J, Briggs J, Xie D, Lai J, Stadlen A, Li B, Fox JA, Presta LG. 2001. High-resolution mapping of the binding site on human IgG1 for FcγRI, Fc gamma RII, FcγRIII, and FcRn and design of IgG1 variants with improved binding to the FcγR. J Biol Chem 276:6591–6604. https://doi.org/10.1074/jbc.M009483200.
30. Jefferis R. 2009. Recombinant antibody therapeutics: the impact of glycosylation on mechanisms of action. Trends Pharmacol Sci 30:356–362. https://doi.org/10.1016/j.tips.2009.04.007.
31. Tao MH, Morrison SL. 1989. Studies of aglycosylated chimeric mouse-human IgG. Role of carbohydrate in the structure and effector functions mediated by the human IgG constant region. J Immunol 143:2595–2601.
32. Teh AY, Maresch D, Klein K, Ma JK. 2014. Characterization of VRC01, a potent and broadly neutralizing anti-HIV MAb, produced in transiently and stably transformed tobacco. Plant Biotechnol J 12:300–311. https://doi.org/10.1111/pbi.12137.
33. Loos A, Gach JS, Hackl T, Maresch D, Henkel T, Porodko A, Bui-Minh D, Sommeregger W, Wozniak-Knopp G, Forthal DN, Altmann F, Steinkellner H, Mach L. 2015. Glycan modulation and sulfoengineering of anti-HIV-1 monoclonal antibody PG9 in plants. Proc Natl Acad Sci U S A 112:12675–-12680. https://doi.org/10.1073/pnas.1509090112.
34. Singh AA, Pooe O, Kwezi L, Lotter-Stark T, Stoychev SH, Alexandra K, Gerber I, Bhiman JN, Vorster J, Pauly M, Zeitlin L, Whaley K, Mach L, Steinkellner H, Morris L, Tsekoa TL, Chikwamba R. 2020. Plant-based production of highly potent anti-HIV antibodies with engineered posttranslational modifications. Sci Rep 10:6201. https://doi.org/10.1038/s41598-020-63052-1.
35. Forthal DN, Gach JS, Landucci G, Jez J, Strasser R, Kunert R, Steinkellner H. 2010. Fc-glycosylation influences Fcγ receptor binding and cell-mediated anti-HIV activity of monoclonal antibody 2G12. J Immunol 185:6876–6882. https://doi.org/10.4049/jimmunol.1002600.
36. Julien JP, Cupo A, Sok D, Stanfield RL, Lyumkis D, Deller MC, Klasse PJ, Burton DR, Sanders RW, Moore JP, Ward AB, Wilson IA. 2013. Crystal structure of a soluble cleaved HIV-1 envelope trimer. Science 342:1477–1483. https://doi.org/10.1126/science.1245625.
37. Julien JP, Sok D, Khayat R, Lee JH, Doores KJ, Walker LM, Ramos A, Diwanji DC, Pejchal R, Cupo A, Katpally U, Depetris RS, Stanfield RL, McBride R, Marozsan AJ, Paulson JC, Sanders RW, Moore JP, Burton DR, Poignard P, Ward AB, Wilson IA. 2013. Broadly neutralizing antibody PGT121 allosterically modulates CD4 binding via recognition of the HIV-1 gp120 V3 base and multiple surrounding glycans. PLoS Pathog 9:e1003342. https://doi.org/10.1371/journal.ppat.1003342.
38. Kong L, Lee JH, Doores KJ, Murin CD, Julien JP, McBride R, Liu Y, Marozsan A, Cupo A, Klasse PJ, Hoffenberg S, Caulfield M, King CR, Hua Y, Le KM, Khayat R, Deller MC, Clayton T, Tien H, Feizi T, Sanders RW, Paulson JC, Moore JP, Stanfield RL, Burton DR, Ward AB, Wilson IA. 2013. Supersite of immune vulnerability on the glycosylated face of HIV-1 envelope glycoprotein gp120. Nat Struct Mol Biol 20:796–803. https://doi.org/10.1038/nsmb.2594.
39. Pejchal R, Doores KJ, Walker LM, Khayat R, Huang PS, Wang SK, Stanfield RL, Julien JP, Ramos A, Crispin M, Depetris R, Katpally U, Marozsan A, Cupo A, Maloveste S, Liu Y, McBride R, Ito Y, Sanders RW, Ogohara C, Paulson JC, Feizi T, Scanlan CN, Wong CH, Moore JP, Olson WC, Ward AB, Poignard P, Schief WR, Burton DR, Wilson IA. 2011. A potent and broad neutralizing antibody recognizes and penetrates the HIV glycan shield. Science 334:1097–1103. https://doi.org/10.1126/science.1213256.
40. Walker LM, Huber M, Doores KJ, Falkowska E, Pejchal R, Julien JP, Wang SK, Ramos A, Chan-Hui PY, Moyle M, Mitcham JL, Hammond PW, Olsen OA, Phung P, Fling S, Wong CH, Phogat S, Wrin T, Simek MD, Protocol GPI, Koff WC, Wilson IA, Burton DR, Poignard P, Protocol Group Principal Investigators. 2011. Broad neutralization coverage of HIV by multiple highly potent antibodies. Nature 477:466–470. https://doi.org/10.1038/nature10373.
41. Moldt B, Rakasz EG, Schultz N, Chan-Hui PY, Swiderek K, Weisgrau KL, Piaskowski SM, Bergman Z, Watkins DI, Poignard P, Burton DR. 2012. Highly potent HIV-specific antibody neutralization *in vitro* translates into effective protection against mucosal SHIV challenge *in vivo*. Proc Natl Acad Sci U S A 109:18921–18925. https://doi.org/10.1073/pnas.1214785109.
42. Hangartner L, Beauparlant D, Rakasz E, Nedellec R, Hoze N, McKenney K, Martins MA, Seabright GE, Allen JD, Weiler AM, Friedrich TC, Regoes RR, Crispin M, Burton DR. 2021. Effector function does not contribute to protection from virus challenge by a highly potent HIV broadly neutralizing antibody in nonhuman primates. Sci Transl Med 13:eabe3349. https://doi.org/10.1126/scitranslmed.abe3349.
43. Parsons MS, Lee WS, Kristensen AB, Amarasena T, Khoury G, Wheatley AK, Reynaldi A, Wines BD, Hogarth PM, Davenport MP, Kent SJ. 2019. Fc-dependent functions are redundant to efficacy of anti-HIV antibody PGT121 in macaques. J Clin Invest 129:182–191. https://doi.org/10.1172/JCI122466.
44. Pauthner MG, Nkolola JP, Havenar-Daughton C, Murrell B, Reiss SM, Bastidas R, Prevost J, Nedellec R, von Bredow B, Abbink P, Cottrell CA, Kulp DW, Tokatlian T, Nogal B, Bianchi M, Li H, Lee JH, Butera ST, Evans DT, Hangartner L, Finzi A, Wilson IA, Wyatt RT, Irvine DJ, Schief WR, Ward AB, Sanders RW, Crotty S, Shaw GM, Barouch DH, Burton DR. 2019. Vaccine-induced protection from homologous tier 2 SHIV challenge in nonhuman primates depends on serum-neutralizing antibody titers. Immunity 50:241–252. https://doi.org/10.1016/j.immuni.2018.11.011.
45. Wang P, Gajjar MR, Yu J, Padte NN, Gettie A, Blanchard JL, Russell-Lodrigue K, Liao LE, Perelson AS, Huang Y, Ho DD. 2020. Quantifying the contribution of Fc-mediated effector functions to the antiviral activity of anti-HIV-1 IgG1 antibodies *in vivo*. Proc Natl Acad Sci U S A 117:18002–-18009. https://doi.org/10.1073/pnas.2008190117.
46. Hessell AJ, Hangartner L, Hunter M, Havenith CE, Beurskens FJ, Bakker JM, Lanigan CM, Landucci G, Forthal DN, Parren PW, Marx PA, Burton DR. 2007. Fc

receptor but not complement binding is important in antibody protection against HIV. Nature 449:101–104. https://doi.org/10.1038/nature06106.
47. Lu CL, Murakowski DK, Bournazos S, Schoofs T, Sarkar D, Halper-Stromberg A, Horwitz JA, Nogueira L, Golijanin J, Gazumyan A, Ravetch JV, Caskey M, Chakraborty AK, Nussenzweig MC. 2016. Enhanced clearance of HIV-1-infected cells by broadly neutralizing antibodies against HIV-1 *in vivo*. Science 352:1001–1004. https://doi.org/10.1126/science.aaf1279.
48. Pietzsch J, Gruell H, Bournazos S, Donovan BM, Klein F, Diskin R, Seaman MS, Bjorkman PJ, Ravetch JV, Ploss A, Nussenzweig MC. 2012. A mouse model for HIV-1 entry. Proc Natl Acad Sci U S A 109:15859–15864. https://doi.org/10.1073/pnas.1213409109.
49. Forthal D, Finzi A. 2019. Blocking HIV-1 replication: are Fc-Fcγ receptor interactions required? J Clin Invest 129:53–54. https://doi.org/10.1172/JCI125264.
50. Ma B, Guan X, Li Y, Shang S, Li J, Tan Z. 2020. Protein glycoengineering: an approach for improving protein properties. Front Chem 8:622. https://doi.org/10.3389/fchem.2020.00622.
51. Montero-Morales L, Steinkellner H. 2018. Advanced plant-based glycan engineering. Front Bioeng Biotechnol 6:81. https://doi.org/10.3389/fbioe.2018.00081.
52. Princiotto AM, Vrbanac VD, Melillo B, Park J, Tager AM, Smith AB, 3rd, Sodroski J, Madani N. 2018. A small-molecule CD4-mimetic compound protects bone marrow-liver-thymus humanized mice from HIV-1 infection. J Infect Dis 218:471–475. https://doi.org/10.1093/infdis/jiy174.
53. Nishimura Y, Gautam R, Chun TW, Sadjadpour R, Foulds KE, Shingai M, Klein F, Gazumyan A, Golijanin J, Donaldson M, Donau OK, Plishka RJ, Buckler-White A, Seaman MS, Lifson JD, Koup RA, Fauci AS, Nussenzweig MC, Martin MA. 2017. Early antibody therapy can induce long-lasting immunity to SHIV. Nature 543:559–563. https://doi.org/10.1038/nature21435.
54. Vogel CL, Cobleigh MA, Tripathy D, Gutheil JC, Harris LN, Fehrenbacher L, Slamon DJ, Murphy M, Novotny WF, Burchmore M, Shak S, Stewart SJ, Press M. 2002. Efficacy and safety of trastuzumab as a single agent in first-line treatment of HER2-overexpressing metastatic breast cancer. J Clin Oncol 20:719–726. https://doi.org/10.1200/JCO.2002.20.3.719.
55. Richard J, Prevost J, Baxter AE, von Bredow B, Ding S, Medjahed H, Delgado GG, Brassard N, Sturzel CM, Kirchhoff F, Hahn BH, Parsons MS, Kaufmann DE, Evans DT, Finzi A. 2018. Uninfected bystander cells impact the measurement of HIV-specific antibody-dependent cellular cytotoxicity responses. mBio 9:e00358-18. https://doi.org/10.1128/mBio.00358-18.
56. Veillette M, Desormeaux A, Medjahed H, Gharsallah NE, Coutu M, Baalwa J, Guan Y, Lewis G, Ferrari G, Hahn BH, Haynes BF, Robinson JE, Kaufmann DE, Bonsignori M, Sodroski J, Finzi A. 2014. Interaction with cellular CD4 exposes HIV-1 envelope epitopes targeted by antibody-dependent cell-mediated cytotoxicity. J Virol 88:2633–2644. https://doi.org/10.1128/JVI.03230-13.
57. Alpert MD, Heyer LN, Williams DE, Harvey JD, Greenough T, Allhorn M, Evans DT. 2012. A novel assay for antibody-dependent cell-mediated cytotoxicity against HIV-1- or SIV-infected cells reveals incomplete overlap with antibodies measured by neutralization and binding assays. J Virol 86:12039–12052. https://doi.org/10.1128/JVI.01650-12.
58. von Bredow B, Arias JF, Heyer LN, Moldt B, Le K, Robinson JE, Zolla-Pazner S, Burton DR, Evans DT. 2016. Comparison of antibody-dependent cell-mediated cytotoxicity and virus neutralization by HIV-1 Env-specific monoclonal antibodies. J Virol 90:6127–6139. https://doi.org/10.1128/JVI.00347-16.
59. Arias JF, Heyer LN, von Bredow B, Weisgrau KL, Moldt B, Burton DR, Rakasz EG, Evans DT. 2014. Tetherin antagonism by Vpu protects HIV-infected cells from antibody-dependent cell-mediated cytotoxicity. Proc Natl Acad Sci U S A 111:6425–6430. https://doi.org/10.1073/pnas.1321507111.
60. Ferrara C, Grau S, Jager C, Sondermann P, Brunker P, Waldhauer I, Hennig M, Ruf A, Rufer AC, Stihle M, Umana P, Benz J. 2011. Unique carbohydrate-carbohydrate interactions are required for high affinity binding between FcγRIII and antibodies lacking core fucose. Proc Natl Acad Sci U S A 108:12669–12674. https://doi.org/10.1073/pnas.1108455108.
61. Wines BD, Vanderven HA, Esparon SE, Kristensen AB, Kent SJ, Hogarth PM. 2016. Dimeric FcγR ectodomains as probes of the Fc receptor function of anti-influenza virus IgG. J Immunol 197:1507–1516. https://doi.org/10.4049/jimmunol.1502551.
62. McLean MR, Madhavi V, Wines BD, Hogarth PM, Chung AW, Kent SJ. 2017. Dimeric Fcγ Receptor enzyme-linked immunosorbent assay to study HIV-specific antibodies: a new look into breadth of Fcγ receptor antibodies induced by the RV144 vaccine trial. J Immunol 199:816–826. https://doi.org/10.4049/jimmunol.1602161.
63. Anand SP, Prevost J, Baril S, Richard J, Medjahed H, Chapleau JP, Tolbert WD, Kirk S, Smith AB, 3rd, Wines BD, Kent SJ, Hogarth PM, Parsons MS, Pazgier M, Finzi A. 2019. Two families of Env antibodies efficiently engage Fc-gamma receptors and eliminate HIV-1-infected Cells. J Virol 93:e01823-18. https://doi.org/10.1128/JVI.01823-18.
64. Davey RT, Jr, Dodd L, Proschan MA, Neaton J, Neuhaus Nordwall J, Koopmeiners JS, Beigel J, Tierney J, Lane HC, Fauci AS, Massaquoi MBF, Sahr F, Malvy D, Prevail II Writing Group, Multi-National Prevail II Study Team. 2016. A randomized, controlled trial of ZMapp for Ebola virus infection. N Engl J Med 375:1448–1456. https://doi.org/10.1056/NEJMoa1604330.
65. Chen Q, Davis KR. 2016. The potential of plants as a system for the development and production of human biologics. F1000Res 5:912. https://doi.org/10.12688/f1000research.8010.1.
66. Strasser R, Stadlmann J, Schahs M, Stiegler G, Quendler H, Mach L, Glossl J, Weterings K, Pabst M, Steinkellner H. 2008. Generation of glyco-engineered *Nicotiana benthamiana* for the production of monoclonal antibodies with a homogeneous human-like N-glycan structure. Plant Biotechnol J 6:392–402. https://doi.org/10.1111/j.1467-7652.2008.00330.x.
67. Shinkawa T, Nakamura K, Yamane N, Shoji-Hosaka E, Kanda Y, Sakurada M, Uchida K, Anazawa H, Satoh M, Yamasaki M, Hanai N, Shitara K. 2003. The absence of fucose but not the presence of galactose or bisecting *N*-acetylglucosamine of human IgG1 complex-type oligosaccharides shows the critical role of enhancing antibody-dependent cellular cytotoxicity. J Biol Chem 278:3466–3473. https://doi.org/10.1074/jbc.M210665200.
68. Houde D, Peng Y, Berkowitz SA, Engen JR. 2010. Posttranslational modifications differentially affect IgG1 conformation and receptor binding. Mol Cell Proteomics 9:1716–1728. https://doi.org/10.1074/mcp.M900540-MCP200.
69. Nimmerjahn F, Anthony RM, Ravetch JV. 2007. Agalactosylated IgG antibodies depend on cellular Fc receptors for *in vivo* activity. Proc Natl Acad Sci U S A 104:8433–8437. https://doi.org/10.1073/pnas.0702936104.
70. Peschke B, Keller CW, Weber P, Quast I, Lunemann JD. 2017. Fc-galactosylation of human immunoglobulin gamma isotypes improves C1q binding and enhances complement-dependent cytotoxicity. Front Immunol 8:646. https://doi.org/10.3389/fimmu.2017.00646.
71. Richard J, Veillette M, Brassard N, Iyer SS, Roger M, Martin L, Pazgier M, Schon A, Freire E, Routy JP, Smith AB, III, Park J, Jones DM, Courter JR, Melillo BN, Kaufmann DE, Hahn BH, Permar SR, Haynes BF, Madani N, Sodroski JG, Finzi A. 2015. CD4 mimetics sensitize HIV-1-infected cells to ADCC. Proc Natl Acad Sci U S A 112:E2687–E2694. https://doi.org/10.1073/pnas.1506755112.
72. Thomann M, Reckermann K, Reusch D, Prasser J, Tejada ML. 2016. Fc-galactosylation modulates antibody-dependent cellular cytotoxicity of therapeutic antibodies. Mol Immunol 73:69–75. https://doi.org/10.1016/j.molimm.2016.03.002.
73. Borducchi EN, Liu J, Nkolola JP, Cadena AM, Yu WH, Fischinger S, Broge T, Abbink P, Mercado NB, Chandrashekar A, Jetton D, Peter L, McMahan K, Moseley ET, Bekerman E, Hesselgesser J, Li W, Lewis MG, Alter G, Geleziunas R, Barouch DH. 2018. Antibody and TLR7 agonist delay viral rebound in SHIV-infected monkeys. Nature 563:360–364. https://doi.org/10.1038/s41586-018-0600-6.
74. Hsu DC, Schuetz A, Imerbsin R, Silsorn D, Pegu A, Inthawong D, Sopanaporn J, Visudhiphan P, Chuenarom W, Keawboon B, Shi W, Robb ML, Mascola JR, Geleziunas R, Koup RA, Barouch DH, Michael NL, Vasan S. 2021. TLR7 agonist, N6-LS and PGT121 delayed viral rebound in SHIV-infected macaques after antiretroviral therapy interruption. PLoS Pathog 17:e1009339. https://doi.org/10.1371/journal.ppat.1009339.
75. Fontaine J, Coutlee F, Tremblay C, Routy JP, Poudrier J, Roger M, Montreal Primary HIVI, Long-Term Nonprogressor Study G, Montreal Primary HIV Infection and Long-Term Nonprogressor Study Groups. 2009. HIV infection affects blood myeloid dendritic cells after successful therapy and despite nonprogressing clinical disease. J Infect Dis 199:1007–1018. https://doi.org/10.1086/597278.
76. Fontaine J, Chagnon-Choquet J, Valcke HS, Poudrier J, Roger M, Montreal Primary HIVI, Long-Term Non-Progressor Study G. 2011. High expression levels of B lymphocyte stimulator (BLyS) by dendritic cells correlate with HIV-related B-cell disease progression in humans. Blood 117:145–155. https://doi.org/10.1182/blood-2010-08-301887.
77. Garabagi F, McLean MD, Hall JC. 2012. Transient and stable expression of antibodies in *Nicotiana* species. Methods Mol Biol 907:389–408. https://doi.org/10.1007/978-1-61779-974-7_23.
78. Grohs BM, Niu Y, Veldhuis LJ, Trabelsi S, Garabagi F, Hassell JA, McLean MD, Hall JC. 2010. Plant-produced trastuzumab inhibits the growth of HER2 positive cancer cells. J Agric Food Chem 58:10056–10063. https://doi.org/10.1021/jf102284f.

79. Timmermans MC, Maliga P, Vieira J, Messing J. 1990. The pFF plasmids: cassettes utilizing CaMV sequences for expression of foreign genes in plants. J Biotechnol 14:333–344. https://doi.org/10.1016/0168-1656(90)90117-T.
80. Castilho A, Beihammer G, Pfeiffer C, Goritzer K, Montero-Morales L, Vavra U, Maresch D, Grunwald-Gruber C, Altmann F, Steinkellner H, Strasser R. 2018. An oligosaccharyltransferase from *Leishmania major* increases the N-glycan occupancy on recombinant glycoproteins produced in *Nicotiana benthamiana*. Plant Biotechnol J 16:1700–1709. https://doi.org/10.1111/pbi.12906.
81. An YQ, McDowell JM, Huang S, McKinney EC, Chambliss S, Meagher RB. 1996. Strong, constitutive expression of the *Arabidopsis* ACT2/ACT8 actin subclass in vegetative tissues. Plant J 10:107–121. https://doi.org/10.1046/j.1365-313x.1996.10010107.x.
82. Strasser R, Castilho A, Stadlmann J, Kunert R, Quendler H, Gattinger P, Jez J, Rademacher T, Altmann F, Mach L, Steinkellner H. 2009. Improved virus neutralization by plant-produced anti-HIV antibodies with a homogeneous β1,4-galactosylated N-glycan profile. J Biol Chem 284:20479–20485. https://doi.org/10.1074/jbc.M109.014126.
83. Almquist KC, McLean MD, Niu Y, Byrne G, Olea-Popelka FC, Murrant C, Barclay J, Hall JC. 2006. Expression of an anti-botulinum toxin A neutralizing single-chain Fv recombinant antibody in transgenic tobacco. Vaccine 24:2079–2086. https://doi.org/10.1016/j.vaccine.2005.11.014.
84. Olea-Popelka F, McLean MD, Horsman J, Almquist K, Brandle JE, Hall JC. 2005. Increasing expression of an anti-picloram single-chain variable fragment (ScFv) antibody and resistance to picloram in transgenic tobacco (*Nicotiana tabacum*). J Agric Food Chem 53:6683–6690. https://doi.org/10.1021/jf0507691.
85. Li H, Wang S, Kong R, Ding W, Lee FH, Parker Z, Kim E, Learn GH, Hahn P, Policicchio B, Brocca-Cofano E, Deleage C, Hao X, Chuang GY, Gorman J, Gardner M, Lewis MG, Hatziioannou T, Santra S, Apetrei C, Pandrea I, Alam SM, Liao HX, Shen X, Tomaras GD, Farzan M, Chertova E, Keele BF, Estes JD, Lifson JD, Doms RW, Montefiori DC, Haynes BF, Sodroski JG, Kwong PD, Hahn BH, Shaw GM. 2016. Envelope residue 375 substitutions in simian-human immunodeficiency viruses enhance CD4 binding and replication in rhesus macaques. Proc Natl Acad Sci U S A 113:E3413–E422. https://doi.org/10.1073/pnas.1606636113.
86. Veillette M, Coutu M, Richard J, Batraville LA, Dagher O, Bernard N, Tremblay C, Kaufmann DE, Roger M, Finzi A. 2015. The HIV-1 gp120 CD4-bound conformation is preferentially targeted by antibody-dependent cellular cytotoxicity-mediating antibodies in sera from HIV-1-infected individuals. J Virol 89:545–551. https://doi.org/10.1128/JVI.02868-14.
87. Richard J, Veillette M, Ding S, Zoubchenok D, Alsahafi N, Coutu M, Brassard N, Park J, Courter JR, Melillo B, Smith AB, 3rd, Shaw GM, Hahn BH, Sodroski J, Kaufmann DE, Finzi A. 2016. Small CD4 mimetics prevent HIV-1 uninfected bystander $CD4^+$ T cell killing mediated by antibody-dependent cell-mediated cytotoxicity. EBioMedicine 3:122–134. https://doi.org/10.1016/j.ebiom.2015.12.004.
88. Weiss MS. 2001. Global indicators of X-ray data quality. J Appl Cryst 34:130–135. https://doi.org/10.1107/S0021889800018227.
89. Karplus PA, Diederichs K. 2012. Linking crystallographic model and data quality. Science 336:1030–1033. https://doi.org/10.1126/science.1218231.
90. Brunger AT. 1997. Free R value: cross-validation in crystallography. Methods Enzymol 277:366–396. https://doi.org/10.1016/s0076-6879(97)77021-6.